YNU
YOKOHAMA National University

TU Graz

# Student Poster Presentation on Hydrogen and Fuel Cells

## within the 15th International Summer School on Advanced Studies of Polymer Electrolyte Fuel Cells

Graz University of Technology, August 30th, 2023

TUAUSTRIA
Austrian Universities of Technology

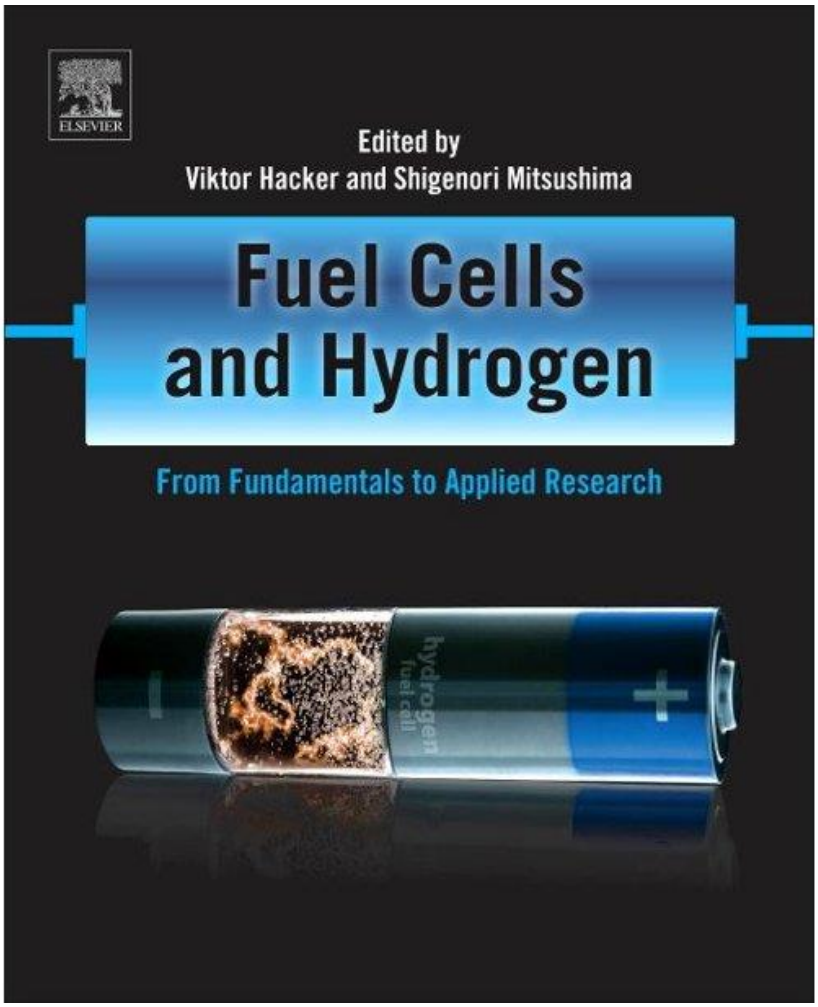


***Fuel Cells and Hydrogen: From Fundamentals to Applied Research***
*Viktor HACKER, Shigenori MITSUSHIMA (eds.)*
*ISBN: 9780128114599, Elsevier 296 pages, 19th July 2018.*

*Fuel Cells and Hydrogen: From Fundamentals to Applied Research* provides an overview of the basic principles of fuel cell and hydrogen technology, which subsequently allows the reader to delve more deeply into applied research. In addition to covering the **basic principles of fuel cells** and hydrogen technologies, the book examines the principles and methods to **develop and test fuel cells**, the evaluation of the **performance** and **lifetime** of fuel cells and the concepts of **hydrogen production**. *Fuel Cells and Hydrogen: From Fundamentals to Applied Research* acts as an invaluable reference book for **fuel cell developers** and **students**, researchers in **industry** entering the area of fuel cells and lecturers teaching fuel cells and hydrogen technology.

# Contents

# Poster Abstracts

# 01 WATER MASS TRANSPORT THROUGH THE POLYMERIC ELECTROLYTE MEMBRANE OF TOLUENE DIRECT ELECTRO-HYDROGENATION ELECTROLYZER

Antonio Atienza-Márquez[1], Takuto Araki[2], and Shigenori MItsuhima[3,4]

[1]Yokohama National University, Institute of Advanced Sciences (IAS), Tokiwadai 79-5, Hodogaya-ku, Yokohama, 240-8501, Japan
[2] Yokohama National University, Faculty of Engineering, Division of Systems Research, 79-5, Hodogaya-ku, Yokohama, 240-8501, Japan
[3] Yokohama National University, Green Hydrogen Research Center, 79-5, Hodogaya-ku, Yokohama, 240-8501, Japan
e-mail: atienza-antonio-zr@ynu.ac.jp

**Keywords:** hydrogen transport, toluene/MCH organic hydride, PEM electrolyzer, direct electro-hydrogenation, water mass transport.

## INTRODUCTION

The organic hydride toluene/methylcyclohexane (MCH) is one of the most promising liquid organic hydrogen carriers (LOHCs) for the bulk and long-distance transport of hydrogen. Its oil-like characteristics allow the use of the existing gasoline infrastructure, and its toxicity is low. Moreover, the direct electro-hydrogenation of the toluene technique, based on proton exchange membrane electrolyzer (PEM) technology (Fig. 1 (a)), has advantages in terms of energy efficiency concerning the conventional two-step and exothermic toluene hydrogenation process [1]. However, in practice, the overall conversion ratio could be lower than 100% and hydrogen gas is generated as a side reaction at the cathode catalyst electrode (Fig. 1 (a)) [2]. A reason is that the toluene path to the reaction site may be partially blocked by the water dragged from the anode side [3], The objective of this research is to study, through experiments and numerical simulation, the water mass transport phenomenon through the polymeric electrolyte membrane of an operating toluene direct electro-hydrogenation electrolyzer under various operating conditions and using diluted sulfuric acid as anode reactant.

## EXPERIMENTAL AND MODELLING

Fig. 1 (b) shows a picture of the experimental 10x10 cm electrolyzer cell used in this study. Nafion® 117 was used as the polymeric electrolyte membrane. The experimental conditions were the following. The electric current was varied between 0.1-0.8 A/cm$^2$; the concentrations of sulfuric acid in the reactant supplied to the anode side, in mol/L, were 0.1, 0.5, 1.0, and 1.5. As for the numerical simulations, a one-dimensional modelling of water transport has been developed in Python. It is assumed that the water transport through the polymeric electrolyte membrane is governed mainly by electro-osmosis (eo) and back diffusion (bd) mechanisms. The total water flux through the membrane ($J_w$) is calculated from the following mathematical expression:

$$J_w = J_{eo} + J_{bd} = n_d \cdot i/\mathrm{F} - D \cdot \rho/\mathrm{EW} \cdot \Delta\lambda \quad (2)$$

where, $n_d$, $i$, F, $D$, ρ, EW and $\lambda$ represent the electro-osmotic coefficient, current density, the Faraday constant, the Fickian water diffusion coefficient, the density and equivalent weight of the membrane, and the water content of the membrane (mol-$H_2O$/mol-$SO_3^-$), respectively.

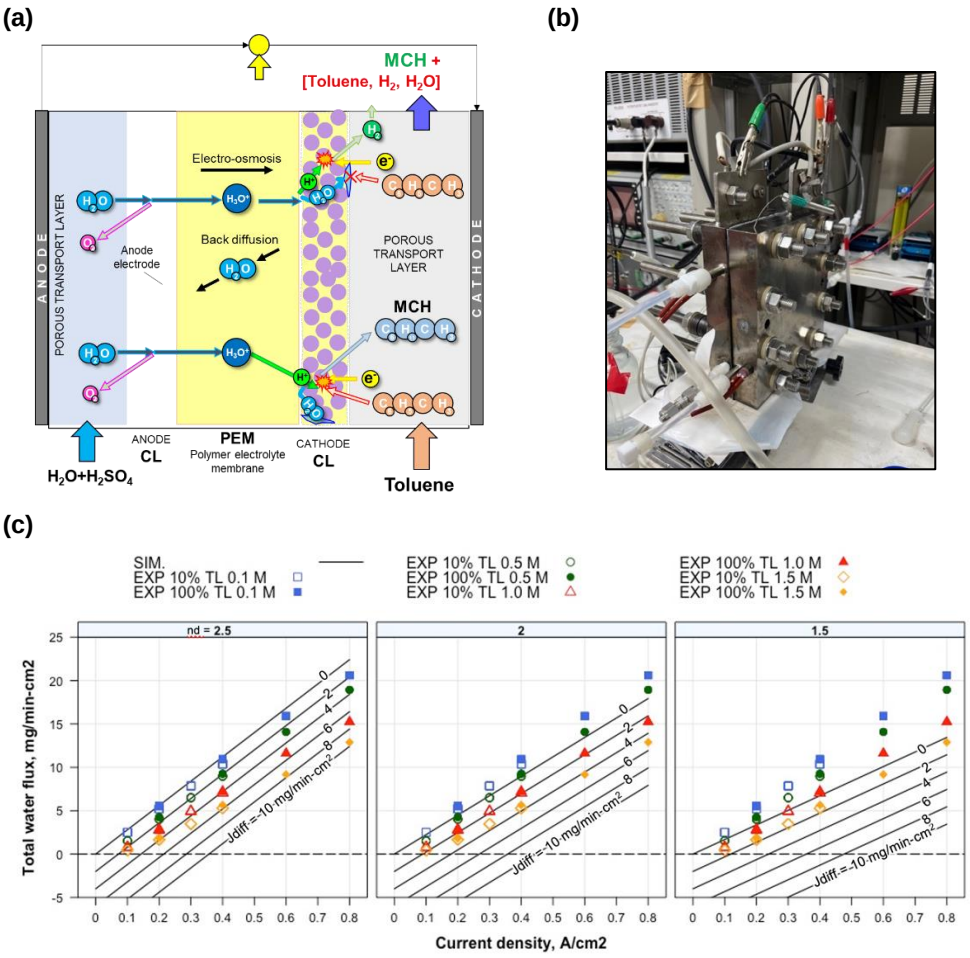


Fig.1. (a) Schematic diagram of a toluene direct electro-hydrogenation PEM-type electrolyzer. (b) Electrolyzer cell used in this study. (c) Preliminary results.

## PRELIMINARY RESULTS

Fig. 1 (c) shows that as the sulfuric acid concentration in the anode reactant increases, the electro-osmotic drag coefficient decrease, and back diffusion flux increases. The thermodynamic activity of the anode reactant decreases with the concentration of sulfuric acid. This could lead to a higher water content gradient, promoting back diffusion and reducing the electro-osmotic drag coefficient of the membrane. The upcoming works will thoroughly analyze the results from experiments and simulations.

## REFERENCES

[1] Shigemasa K, Atienza-Márquez A, et al. J Power Sources 2023; 554: 232304.
[2] Nagasawa K, Sugita Y, Atienza-Márquez A, Kuroda Y, Mitsushima S. Journal of Electroanalytical Chemistry 2023:117431
[3] F.I. Reyna-Peña, A. Atienza-Márquez, et al. International Journal of Hydrogen Energy (accepted for publication). Manuscript No. HE-D-23-04353R1

# 02 *IN SITU* FORMATION OF NON NOBLE METAL NANOPARTICLES IN A POLYMER DERIVED HIGH SPECIFIC SURFACE AREA SI-C-N-O(H) SUPPORT TO PROMOTE ELECTROCATALYTIC WATER OXIDATION

Marwan Ben Miled[1,2], Stéphane Célérier[2], Aurélien Habrioux[2], Olivier Masson[1], Samuel Bernard[1]

[1]Univ. Limoges, CNRS, IRCER, UMR7315, F-87000 Limoges, France
[2]IC2MP, Université de Poitiers, CNRS, F-86073 Poitiers, France

**Keywords:** PDC, non-noble metals, nanoparticles, water electrolysis

Hydrogen is considered as a promising energy carrier to assure the needs of humanity. Its combustion in a fuel cell (FC) emits only water and does not involve any noise pollution. The use of H2 in a fuel cell requires it to be obtained at a very high level of purity, which can be easily achieved by water electrolysis. This process i) uses noble metal catalysts that are difficult to substitute in the PEM technologies that are currently the most mature for low temperature electrolysis, ii) has limited electrical performance due to anode overpotential. The recent development of anion exchange membrane materials has led to the emergence of a new technology: the anion exchange membrane electrolyser. This device allows the use of non-noble transition metals in the composition of catalysts for hydrogen (HER) and oxygen (OER) evolution reactions in alkaline media. However, their nanoscaled synthesis is highly challenging to limit the overpotential, particularly at the anode (OER); one of the half-reaction of water electrolysis is involving a four-electron transfer hampered by kinetic factors.
The PDC (Polymer Derived Ceramics) route is a way to generate ceramics from pre-ceramic polymers used as precursors. Organosilicon polymers are usually used as pre-ceramic polymers. Their backbone represents a highly reactive platform to link or coordinate lower-molecular weight TM complexes. Thus, the as-obtained pre-ceramic polymer will promote upon heat-treatment, in general at low temperature, the precipitation of well dispersed transition metal nanoparticles in an amorphous Si-C-O-N ceramic because of the strong reducing properties of organosilicon polymers. Having in mind that pre-ceramic polymers display an intrinsic ability to form micropores in the low-temperature regime of the thermolysis, the resulting nanocomposites produced at low temperature are expected to : (i) display long-term stability due to stronger nanoparticle-matrix interaction and high corrosion resistance of the matrix; (ii) expose and access more active sites ; (iii) avoid active sites aggregation during electrochemical process leading thereby to a constant catalytic activity; and (iv) have practical applicability. This poster will discuss on recent works obtained in the framework of the SYNERGY project between IRCER and IC2MP. They are based on the implementation of the PDC route to in situ form Ni nanoparticles in an amorphous Si-C-N-O(H) ceramic support at low temperatures (300-700 °C). The large specific surface area of the materials associated with the nanometric size (20-50 nm) of the Ni particles made it possible to boost OER performances, which suggests very promising prospects for the development of anion exchange membrane electrolysers [1].

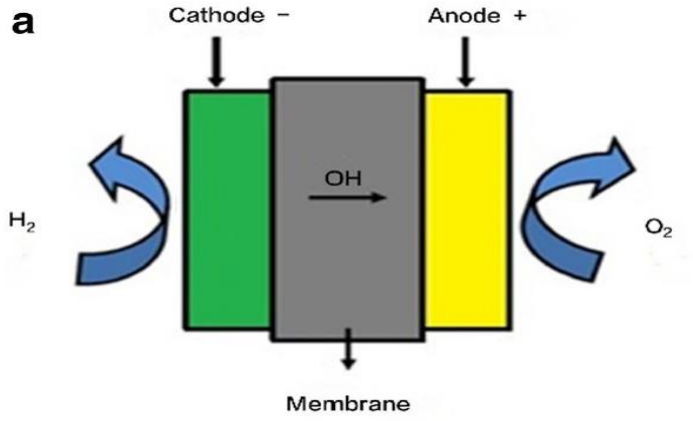


Fig 1: Anion exchange membrane for water electrolysis in alkaline media [2]

REFERENCES

[1] R. K. M. Ferreira, M. Ben Miled, R. K. Nishihora, N. Christophe, P. Carles, G. Motz, A. Bouzid, R. Machado, O. Masson, Y. Iwamoto, S. Célérier, A. Habrioux, S. Bernard, accepted in Nanoscale. Adv., 2023

[2] M. A. Khan, H. Zhao, W. Zou, Z. Chen, W. Cao, J. Fang, J. Xu, L. Zhang and J. Zhang, Electrochem. Energ. Rev., 2018, 1, 483–530

# 03 COMPARISON OF THE DOMINANT LOW TEMPERATURE WATER ELECTROLYSIS TECHNOLOGIES

Florian de Pauli[1], Matthias Ranz[1], Alexander Trattner[1], Viktor Hacker[2]

[1]Hydrogen Research Center Austria, Inffeldgasse 17, 8010 Graz, Austria
[2]Graz University of Technology, Institute of Chemical Engineering and Environmental Technologies, Inffeldgasse 25C, 8010 Graz, Austria
e-mail: florian.depauli@student.tugraz.at

**Keywords:** alkaline water electrolysis; proton exchange membrane water electrolysis; anion exchange membrane water electrolysis; polarisation curve; electrochemical impedance spectroscopy

In the current low temperature electrolyser market there are 3 prominent and promising electrolysis technologies: Polymer Exchange Membrane water electrolysis (PEMWE), Alkaline liquid water electrolysis (AELWE) and Anion exchange membrane water electrolysis (AEMWE). All of these technologies have their unique advantages and disadvantages, operation conditions and difficulties. Therefor the end users preferences regarding electrolyte handling, capital expenditure, efficiency and many more need to be considered. Additionally this allows for development inspired by the rivalling technologies and transferable problem solving approaches.[1]
The main differences between the technologies are the used materials and electrolytes.
The high ionic conductivity of the perflurosulfonicacid (PFSA) based polymer membranes used in PEMWEs allow for the usage of pure water as feed, whereas the alkaline systems need to use KOH as feed, however the lower stability of the anion exchange membranes only allow for the usage of 1 M KOH compared to the 6 M used in traditional alkaline water electrolysis. Due to the higher ionic conductivity of the anion exchange membrane compared to the separator material the drawback of using lower electrolyte concentrations is mitigated.
Due to the harsh environment in the PEMWEs, especially on the anode, only platinum group metals can be used as catalysts. Compared to the nickel catalysts that are used in alkaline electrolysis this leads to better catalytic performance but at significantly higher costs. [1-3]
There has been plenty of data reported on the respective technologies, however it is always difficult to compare data from different publishers [1-2]. Therefor the goal and outlook of this study was the characterisation of all technologies in an as equal as possible set up. The same cell design, testing procedure and test bench was used. Due to the different requirements of the technologies, different electrolytes and temperatures had to be used in order to represent state of the art operations.

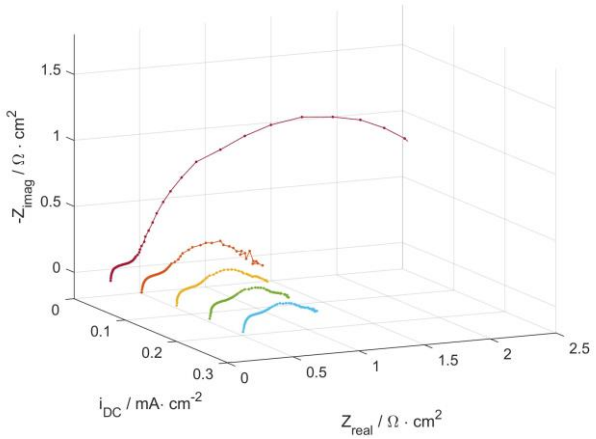


Figure 1: Nyquist Plot at current densities from 50-250 mA/cm2 .

The cell performance was evaluated by obtaining electrochemical impedance spectra at current densities between 50 – 250 mA/cm$^2$, as presented in fig. 1, as well as 100 – 600 mA/cm$^2$, and polarization curves at current densities between 5 - 250 mA/cm2, as well as 10 – 600 mA/cm$^2$, as presented in fig.2. The half-cell reactions were simultaneously investigated with a reversible hydrogen reference electrode. This allows for the allocation of overpotentials, degradation and improvement phenomena to the respective electrodes.

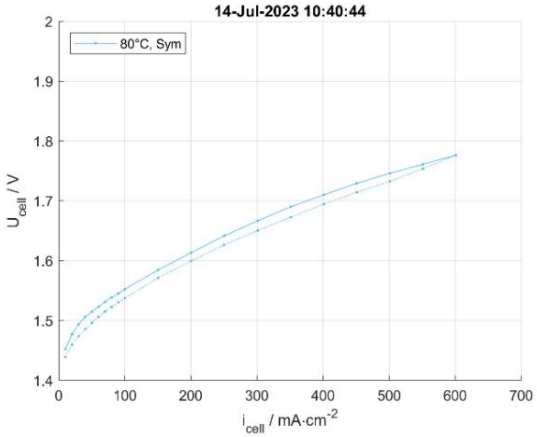


Figure 2: Polarization curve at current densities from 10 – 600 mA/cm$^2$.

REFERENCES

[1] B.Pollet, H.Schäfer; Water Electrolysis: from textbook knowledge to the latest scientific strategies and industrial developments Chem. Soc. Rev., 2022,51, 4583-4762.

[2] A.Butler, H.Spliethoff; Current status of water electrolysis for energy storage, grid balance and sector coupling via power to gas and power to liquids: A review; In: Renewable and Sustainable Energy Reviews 82 (2018), pp. 2440–2454.

[3] Martín David, Carlos Ocampo-Martínez, and Ricardo Sánchez-Peña. “Advances in alkaline water electrolyzers: A review”. In: Journal of Energy Storage 23 (2019), pp. 392–403.

# 04 IMPACT OF TEMPERATURE AND RELATIVE HUMIDITY ON ELECTROCATALYST DEGRADATION IN POLYMER ELECTROLYTE FUEL CELLS: AN EXPERIMENTAL STUDY

Joel Mata Edjokola, Viktor Hacker and Merit Bodner

Working Group Fuel Cell and Hydrogen, Institute of Chemical Engineering and Environmental Technology, Graz University of Technology, 8010 Graz, Austria
e-mail: joel.edjokola@tugraz.at

**Keywords:** catalyst layer, degradation, temperature, relative humidity.

INTRODUCTION

The catalyst layer, which is crucial for efficient electrochemical reactions within the PEFC, undergoes degradation. This leads to a decline in its electrochemical activity and, negatively impacting power output, durability and cost-effectiveness [1–3]. This study utilized an accelerated stress test methodology recommended by the US Department of Energy [4] to investigate the degradation mechanisms influenced by temperature and relative humidity. A single cell was subjected to controlled accelerated aging conditions simulating a realistic operating environment. The reference condition consisted of a cell temperature of 80°C and gas relative humidity of 100%. In addition to the reference condition, two other conditions were evaluated: a cell temperature of 90 °C with 100% gas relative humidity and a cell temperature of 80 °C with 50% gas relative humidity. Various electrochemical techniques, including cyclic voltammetry, polarization curves, and electrochemical impedance spectroscopy, were employed to comprehensively characterize the catalyst layer's behaviour. The experimental results demonstrated the significant influence of temperature and relative humidity on the degradation of the catalyst layer in PEFCs Figure 1 Elevated temperatures accelerated the degradation process, leading to a decrease in the electrochemically active surface area (ECSA) of the catalyst and subsequent decline in fuel cell performance. The findings emphasize the importance of managing these operating parameters to ensure the long-term stability and efficiency of PEFCs.

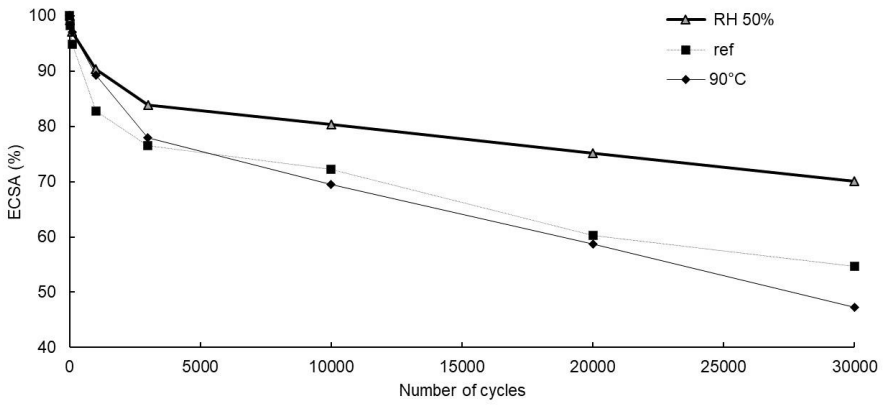


Figure 1:Normalized ECSA loss measured during the accelerated stress test.

ACKNOWLEDGMENT

This research work is performed under the project AlpeDHues (AlpeDHues / FFG 889328) which is supported by the Austrian Research Promotion Agency (FFG).

REFERENCES

[1] Khedekar K, Rezaei Talarposhti M, Besli MM, Kuppan S, Perego A, Chen Y et al. Probing Heterogeneous Degradation of Catalyst in PEM Fuel Cells under Realistic Automotive Conditions with Multi Modal Techniques. Adv. Energy Mater. 2021;11(35):2101794. https://doi.org/10.1002/aenm.202101794.

[2] Okonkwo PC, Ige OO, Barhoumi EM, Uzoma PC, Emori W, Benamor A et al. Platinum degradation mechanisms in proton exchange membrane fuel cell (PEMFC) system: A review. International Journal of Hydrogen Energy 2021;46(29):15850–65. https://doi.org/10.1016/j.ijhydene.2021.02.078.

[3] Jie Song, Qing Ye, Kun Wang, Zhiyuan Guo and Meiling Dou. Degradation Investigation of Electrocatalyst in Proton Exchange Membrane Fuel Cell at a High Energy Efficiency. Molecules 2021(26). https://doi.org/10.3390/molecules26133932.

[4] Harting and Karen. Fuel Cell Technical Team Roadmap 2017

# 05 INVESTIGATION OF THE INFLUENCE OF CARBON DEPOSITION ON THE PURITY OF THE HYDROGEN PRODUCTION IN THE CHEMICAL LOOPING PROCESS

Katharina Halper[1], Fabio Blaschke [1], Michael Lammer[1,2], and Viktor Hacker[1]

[1]Working Group Fuel Cells and Hydrogen, Institute of Chemical Engineering and Environmental Technology Graz University of Technology, Inffeldgasse 25/C/EG, 8010 Graz, Austria
[2]BEST - Bioenergy and Sustainable Technologies GmbH, Inffeldgasse 21b 8010 Graz Austria
e-mail: katharina.halper@tugraz.at

**Keywords:** chemical looping hydrogen, hydrogen production, carbon deposition, oxygen carrier

Today, more than 99% of hydrogen is produced from coal (23%) and natural gas (76%). Less than 0.1% of the hydrogen produced annually is obtained by electrolysis and is mainly used for applications requiring 99.999% hydrogen purity [1]. To achieve the Austrian federal government's goal of making Austria climate neutral by 2040, one focus is on the hydrogen strategy with the guiding principle of improving and supporting technologies and infrastructure for green hydrogen [2]. An alternative and more cost-efficient technology to water splitting with electricity for the decentralized production of green hydrogen is the chemical looping process (CL). An extended form of the CL process is the Reformer Steam Iron Cycle (RESC) with an integrated reformer section. In the reformer section renewable hydrocarbons are converted to syngas, containing $H_2$ and CO. The syngas is transferred to the steam iron section to reduce an iron-based oxygen carrier (OC) following Equation 1. In a subsequent step, the OC is oxidised with steam by yield pure hydrogen according to Equation 2 [3]. A drawback of the process is the deposition of carbon on the OC resulting in $CO_2$ and CO contamination of the product gas. Carbon deposition occurs during the reduction and is described by the Boudouard equilibrium (Equation 3) [4]. In the oxidation step solid carbon is oxidised to $CO_2$ leading to a contaminated product gas stream (Equation 4).

Reduction reaction: $Fe_3O_4 + 4\,H_2/CO \rightarrow 3\,Fe + 4\,H_2O/CO_2$ (1)

Oxidation reaction: $3\,Fe + 4\,H_2O \rightarrow Fe_3O_4 + 4\,H_2$ (2)

Carbon deposition: $CO_2 + C \rightleftharpoons 2\,CO$ (3)

Carbon oxidation: $C + 2\,H_2O \rightarrow CO_2 + 2\,H_2$ (4)

The aim of this work was to investigate the carbon deposition with the associated formation of impurities of the product gas in the hydrogen gas in the CLH process from CO as part of the reduction gas. Therefore, to investigate these phenomena, a reaction setup of a fixed-bed CLH process was designed and built. The experimental setup is schematically presented in Figure 1.

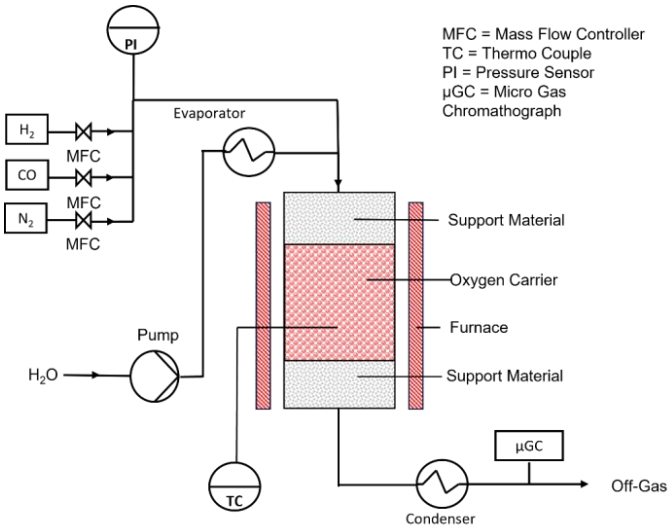


**Figure 1: Schematic presentation of the CLH fixed bed setup for testing the carbon deposition**

Pellets of $Fe_2O_3/Al_2O_3$ in the weight ratio of 80:20 wt.-% with a size of 2 – 4 mm were synthesized and tested for 10 cycles at 800 °C. A hydrogen purity of 99.9% was achieved in all cycles. $CO_2$ was detected as main impurity in the $H_2$ generation. Nevertheless, the study shows the impurities come from the carbon deposition in the reduction cycle followed by an oxidation with water, which leads to the formation of $CO_2$ in the hydrogen stream. Nevertheless, a hydrogen purity of 99.9 vol.% was achieved. It also shows that the reaction setup and the influence of the process parameters on the OC could be investigated. Finally, the research shows, that high purity hydrogen can be produced, and the reaction setup serves as valuable design for further material screening and for investigation of industrial scale up.

ACKNOWLEDGEMENTS

Financial support by the Austrian Research Promotion Agency (FFG) through the 30th Bridge Call and the project BIO-LOOP within the framework of the COMET - Competence Centers for Excellent Technologies program supported by the Federal Ministry for Climate Action, Environment, Energy, Mobility, Innovation, and Technology (BMK), the Federal Ministry for Digital and Economic Affairs (BMDW), and the Province of Styria (SFG) is gratefully acknowledged.

REFERENCES

[1] F. Blaschke, M. Bele, B. Bitschnau, and V. Hacker, “The effect of microscopic phenomena on the performance of iron-based oxygen carriers of chemical looping hydrogen production,” Appl. Catal. B Environ., vol. 327, p. 122434, Jun. 2023, doi: 10.1016/J.APCATB.2023.122434.

[2] I. und T. Bundesmininsterium für Klimaschutz, Umwelt, Mobilität, “Wasserstoffstrategie für Österreich - Executive Summary,” [Online]. Available: https://www.bmk.gv.at/themen/energie/energieversorgung/wasserstoff/strategie.html.

[3] V. Hacker, “A novel process for stationary hydrogen production: the reformer sponge iron cycle (RESC),” J. Power Sources, vol. 118, pp. 311–314, 2003.

[4] S. Bock, R. Zacharias, and V. Hacker, “Experimental study on high-purity hydrogen generation from synthetic biogas in a 10 kW fixed-bed chemical looping system,” RSC Adv., vol. 9, no. 41, pp. 23686–23695, 2019, doi: 10.1039/c9ra03123e.

# 06 EX-SITU MEASUREMENT OF CHEMICAL MEMBRANE DEGRADATION USING PHOTOMETRY

Mathias Heidinger[1], Eveline Kuhnert[1], Kurt Mayer[1], Daniel Sandu[2], Viktor Hacker[1], and Merit Bodner[1]

[1]Graz University of Technology, Institute of Chemical Engineering and Environmental Technologies, Inffeldgasse 25C, 8010 Graz, Austria
[2]AiDEXA GmbH, Bergmanngasse 45 T10, 8010 Graz, Austria
e-mail: mathias.heidinger@tugraz.at

## INTRODUCTION

Despite the critical role that degradation of the perfluorinated sulfonic acid (PFSA) membrane plays in polymer electrolyte fuel cells (PEFCs), it can so far not be reliably and quickly detected through in-situ characterization methods. To complement in-situ, ex-situ measurement methods are available and can partially be conducted while the cell is in operation. Polymer fragments and fluoride from the degradation of the membrane can be found in the effluent water, leaving the fuel cell [1]–[3]. While it is possible to measure membrane degradation outside of the cell, the existing methods have drawbacks or prerequisites on their own. Therefore, the measurement of membrane degradation is proposed using fluoride as the indicator with a zirconium complex (zirco-nyl-2-(4-sulphophenylazo)-1,8-dihydroxy-3,6-naphtalene-disulfonic acid), referred to as SPADNS [4]. The interaction between the complex and fluoride is measured using a photometric method and the quantification is based on the color and intensity shift, caused by the interaction of fluoride with the complex. We find that this method can quantify the fluoride concentration correctly. A comparison to a fluoride-sensitive electrode is conducted and validated using a Bland–Altman correlation. The photometric method also requires smaller sample quantities, reducing the required sample amount to 0.9 ml compared to the 5 to 15 ml required for fluoride-sensitive electrode measurements. Measurement times are also reduced to 60 s per sample, reducing the needed time by more than a factor of 10, compared to measurements with an electrode or through ion chromatography. With this, it is possible to get a complementary information about the state of health of the membrane faster and quantify chemical degradation ex-situ. Chemical membrane degradation can be characterized reliably and in a reasonable timeframe using the proposed method.

## ACKNOWLEDGEMENTS

This research is performed under the HyLife project (K-Project HyTechonomy, FFG grant number 882510) which is supported by the Austrian Research Promotion Agency (FFG).

## REFERENCES

[1] M. Bodner, B. Cermenek, M. Rami, and V. Hacker, “The Effect of Platinum Electrocatalyst on Membrane Degradation in Polymer Electrolyte Fuel Cells,” Membr. 2015, Vol. 5, Pages 888-902, vol. 5, no. 4, pp. 888–902, Dec. 2015, doi: 10.3390/MEMBRANES5040888.

[2] M. A. Yandrasits, A. Komlev, K. Kalstabakken, M. J. Kurkowski, and M. J. Lindell, “Liquid Chromatography/Mass Spectrometry Analysis of Effluent Water from PFSA Membrane Fuel Cells Operated at OCV,” J. Electrochem. Soc., vol. 168, no. 2, p. 024517, Feb. 2021, doi: 10.1149/1945-7111/ABE56A.

[3] M. Bodner, B. Marius, A. Schenk, and V. Hacker, “Determining the Total Fluorine Emission Rate in Polymer Electrolyte Fuel Cell Effluent Water,” ECS Meet. Abstr., vol. MA2017-02, no. 34, p. 1465, Sep. 2017, doi: 10.1149/MA2017-02/34/1465.

[4] M. Heidinger, E. Kuhnert, K. Mayer, D. Sandu, V. Hacker, and M. Bodner, “Photometric Method to Determine Membrane Degradation in Polymer Electrolyte Fuel Cells,” Energies 2023, Vol. 16, Page 1957, vol. 16, no. 4, p. 1957, Feb. 2023, doi: 10.3390/EN16041957.

# 07 ENHANCING WATER ANALYSIS FOR IMPROVED PERFORMANCE AND DURABILITY OF FUEL CELL-POWERED ELECTRIC VEHICLES

Maximilian Käfer[1], Viktor Hacker[1], and Merit Bodner[1]

[1][6670] Institute of Chemical Engineering and Environmental Technology, Graz University of Technology, Inffeldgasse 25/C/EG, 8010 Graz, Austria

**Keywords**: fuel cell-powered electric vehicles, degradation, product water analysis, water management, flooding

## INTRODUCTION

Fuel cell-powered electric vehicles (FCEVs) are gaining increasing interest as a sustainable transportation solution. To achieve faster market penetration and address the challenges faced by FCEVs, significant improvements in their economy, attractiveness, energy efficiency, cost reduction, and durability are necessary. This work focuses on understanding and preventing degradation in FCEVs, with a particular emphasis on the analysis of product water and water management. Water management is a critical aspect of fuel cell technology, playing a vital role in ensuring optimal system performance. Insufficient water management can disrupt the functioning of the system and worsen fuel cell dehydration. Therefore, it is crucial to implement effective strategies for managing water to promote smooth operation and enhance fuel cell efficiency [1]. The current water management practices encounter several challenges at various stages, from the fuel cell itself to the entire fuel cell system. A portion of the water at the fuel cell outlet is redirected for humidifying the feed gases. However, the gas that undergoes anode recirculation has a high dew point, which can result in condensation at the anode when mixed with a gas stream at a lower temperature [2]. Excessive water production can accumulate within the flow channels, as well as the cathode and anode regions. Submerging either the cathode or anode in an excessive amount of water can lead to fuel cell failure [3–5]. Flooding phenomena, characterized by blockages in the flow fields and gas diffusion layers, can cause severe degradation. This leads to fuel starvation, carbon support corrosion, and catalyst degradation [6–8]. Although the inclination of the system can impact flooding, partial condensation is generally tolerable and not measured or quantified. On the other hand, insufficient water content impedes the fuel cell's optimal functioning. These challenges related to water management can be categorized as overflow and dehydration [5]. The voltages during system initiation and idle states can initiate the production of hydrogen peroxide and its corresponding radicals. These radicals possess the capability to break down the membrane, leading to the release of fluoride emissions [7,9].

To address the issues above, this work is set to utilize an open multi-functional modular system as the foundation for further investigations. The exhaust path integrated with a product water sensor should be used to enable the development of a fluoride detection sensor to assess the health of the membrane. Potential strategies for optimizing water management include incorporating heatable optical windows to monitor water transport in the recirculation path and employing optical cells with spectroscopic methods to quantify the presence of liquid water. The findings and optimizations derived from laboratory tests should then be applied to real-world scenarios, particularly in vehicles.

## ACKNOWLEDGEMENT

This project is funded by the Climate and Energy Fund and is carried out within the framework of the programme “Zero Emission Mobility”.

REFERENCES


[1] Yang, Z.; Du, Q.; Jia, Z.; Yang, C.; Jiao, K. Effects of operating conditions on water and heat management by a transient multi-dimensional PEMFC system model. Energy 2019, 183, 462–476.

[2] Liu Z., Chen J., Liu H., Yan C., Hou Y., He Q., Zhang J., Hissel D. Anode purge mamangement for hydrogen utilization and stack durability improvement of PEM fuel cell systems. Applied Energy 2020, 275, 115110.

[3] Fluckiger R., Tiefenauer A., Ruge M., Aebi C., Wokaun A., Buchi F. N. Thermal analysis and optimization of a portable, edge-air-cooled PEFC stack. J Power Sources 2007, 172, 324–333.

[4] Wu J., Galli S., Lagana I., Pozio A., Monteleone G., Yuan X. Z., et al. An air-cooled proton exchange membrane fuel cell with combined oxidant and coolant flow. J Power Sources 2009, 188, 199–204.

[5] Wang, X. R.; Ma, Y.; Gao, J.; Li, T.; Jiang, G. Z.; Sun, Z. Y. Review on water management methods for proton exchange membrane fuel cells. International Journal of Hydrogen Energy 2021, 46, 12206–12229.

[6] Bodner M., Hohenauer C., Hacker V. Effect of pinhole location on degradation in polymer electrolyte fuel cells. Journal of Power Sources 2015, 295, 336–348.

[7] Bodner M., R. M.; Marius B. Determining Membrane Degradation in Polymer Electrolyte Fuel Cells by Effluent Water Analysis. ECS Transactions 2016, 75, 703–706.

[8] Hacker V., M. S. Fuel Cells and Hydrogen - From Fundamentals to Applied Research.

[9] Bodner M., Cermenek B., Rami M. The effect of Platinum Electrocatalyst on Membrane Degradation in Polymer Electrolyte Membrane Fuel Cells. Membranes 2015, 5, 888–902.

# 08 NUMERICAL ANALYSIS CONSIDERING METHANATION REACTION RATES IN AN INTEGRATED SOEC CO-ELECTROLYTIC CELL

Ryosuke Kawanaka[1], Takuto Araki[2]

[1]Grad. Sch. of Eng. Sci., Yokohama National Univ., Tokiwadai 79-5, Hodogaya-ku, Yokohama, Kanagawa pref., Japan
[2] Faculty of Eng., Yokohama National Univ., Tokiwadai 79-5, Hodogaya-ku, Yokohama, Kanagawa pref., Japan
e-mail: kawanaka-ryosuke-jt@ynu.jp

**Keywords:** methanation, reaction rate, SOEC co-electrolytic

## INTRODUCTION

In recent years, efforts have been made around the world to address environmental issues such as global warming, one of which is the reduction of greenhouse gas emissions such as carbon dioxide. To achieve this, it is necessary to decarbonize both the electric power sector, such as thermal power generation, and the heat sector, which accounts for approximately 60% of Japan's industrial and consumer sector energy consumption. The means to address these issues include expanding the use of electricity from renewable energy sources such as photovoltaic and wind power generation, and converting them into gaseous fuels such as hydrogen and methane. Methane, in particular, is the main component of natural gas and can be a high value-added gaseous fuel in that it can be used with existing transportation infrastructure and consumption equipment. Based on our previous results [1], we have numerically confirmed that a cylindrical solid oxide electrolysis cell (SOEC) can produce methane with high efficiency and purity. The system we have investigated features integrated co-electrolysis of feed gas and methane synthesis inside the SOEC, which may lead to system simplification and improved efficiency compared with systems in which co-electrolysis in the SOEC and methane synthesis outside the cell are carried out separately. On the other hand, the integrated system requires a high-pressure state of about 10 atm inside the cell to produce high-purity methane, and there remains a major issue of gas sealing. Based on the above, the objective of this study was to produce high-purity methane at atmospheric pressure inside and outside the cell. For this purpose, we measured the catalyst performance under low-temperature conditions (minimum temperature of 150 °C), where methane production is predominant in terms of chemical equilibrium, and applied the results to numerical analysis. The feasibility of the system was also evaluated by confirming the conditions under which high-purity methane could be produced.

## ANALYSIS METHOD

In this analysis, a small cylindrical SOEC model with a cathode Ni-YSZ support shown in Figure 1 was used. YSZ was used as the electrolyte and an LSM-YSZ mixture was used as the anode, and the area surrounded by the purple and yellow lines in the figure was used as the computational range. First, a temperature field was applied to the entire cell to obtain the current density distribution inside the cell. Next, the electrolytic volume of each grid is calculated using the obtained current density, and the proportion of each material is obtained by equilibrium calculation. The temperature of each grid is then determined, taking into account the amount of heat transported by convection and the amount of heat generated by each reaction. The results of the analysis are obtained by repeating the equilibrium calculations and heat quantity calculations.

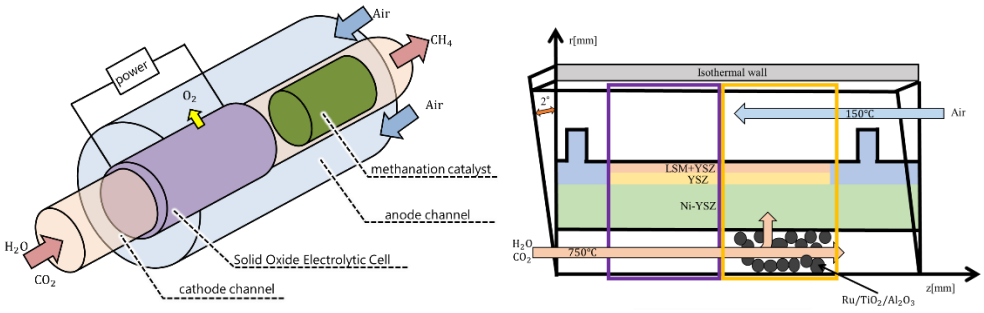


Fig.1 Analysis Model

## RESULTS AND DISCUSSION

As shown in Figure 2, the analysis results confirm that the cathode gas is cooled by changing the anode flow rate and that the temperature distribution changes. It was also found that the methanation reaction reached equilibrium for the designed cell size.

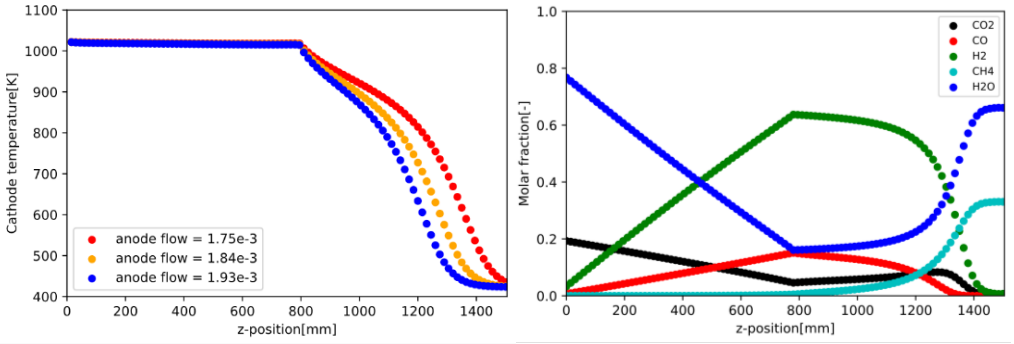


Fig.2 Temperature distribution and mole fraction distribution

## CONCLUSION

In this study, a system that simultaneously performs co-electrolysis and methanation inside a SOEC cell is discussed using numerical analysis. Experimental values for the reaction rate of the methanation catalyst, which is necessary for the analysis, were incorporated into the analysis. As a result, it was found that equilibrium was reached for the reaction rate. It was also found that the cathode gas temperature and mole fraction distribution were affected by changes in anode flow rate.

## REFERENCES

[1] Takuto Araki, Shunki Kawamura, Atsuhito Ota, Energy and Power 70 (294), 29-38, (2020)

# 09 STORAGE EFFECTS OF CATALYST INK FOR POLYMER ELECTROLYTE FUEL CELLS

Mario Kircher[1], Michaela Roschger[1], Wai Yee Koo[2], Fabio Blaschke[1], Maximilian Grandi[1], and Viktor Hacker[1]

[1]Institute of Chemical Engineering and Environmental Technology, Graz University of Technology, Inffeldgasse 25/C, A-8010 Graz
[2]UTP Universiti Teknologi Petronas, Persiaran UTP, 32610 Seri Iskandar, Perak, Malaysia
e-mail: mario.kircher@tugraz.at

About 90% of the energy demand in the transport sector is covered by petroleum products today [1]. A viable way to reduce greenhouse gas emissions in this sector is the use of hydrogen as a fuel for fuel cell vehicles (FCVs). The widespread commercialisation of FCVs demands an increase in reliability and durability as well as a reduction in costs [2,3].

The performance-determining core unit of a polymer electrolyte fuel cell (PEFC), the membrane electrode assembly, consists of a polymer membrane sandwiched between the anodic and cathodic catalyst layers (CLs). CLs are formed by applying catalyst inks (CI) onto the polymer electrolyte membrane e.g., via ultrasonic spray coating or inkjet printing. Most commonly, the CI consists of a catalyst (e.g. platinum), an ionomer as binder and an alcohol-water mixture as solvent. The electrochemical reactions take place in the CL and consequently the CI of the CL is vital for the performance of a PEFC. It has been observed that ageing effects during storage of CI prior to processing into CL lead to the formation of unwanted by-products, activity losses and performance degradation.

This work investigates the effects of ageing of CI over a storage period of up to four weeks. The composition of the CI (Pt/C, Nafion, isopropanol, water) was optimised and is kept constant for all measurements. Sedimentation studies reveal a significant change in concentration of the components over time despite the overall adequate stability of the dispersion. Degradation products formed by the oxidation of isopropanol are qualified and quantified. Results show their non-negligible presence even in freshly prepared CI. Half and fuel cell measurements are used to determine the effect of storage on the catalytic activity and hence, the cell performance. The results of these test series can be used for considerations about CI preparation and storage in small and large-scale PEFC production e.g. to reduce waste or increase PEFC performance.

INTRODUCTION

[1] U.S. Energy Information Administration. Use of energy explained: Energy use for transportation. 2021. URL: https://www.eia.gov/energyexplained/use-of-energy/transportation.php (accessed: 11/04/2022)

[2] Iain Staffell et al. “The role of hydrogen and fuel cells in the global energy system”. In: Energy & Envi-ronmental Science 12 (2019), pp. 463 – 491. DOI: 10.1039/C8EE01157E

[3] Gregory Trencher. “Strategies to accelerate the production and diffusion of fuel cell electric vehicles: Experiences from California”. In: Energy Reports 6 (2020), pp. 2503 - 2519. DOI: 10.1016/j.egyr.2020.09.008

# 10 VISUALIZATION OF MICROSCALE DROPLETS FREEZING ON HYDROPHILIC AND HYDROPHOBIC COMPOSITE SURFACES

Sota Kishi[1], Takuto Araki[2]

[1]Grad. Sch. Of Eng. Sci., Yokohama National Univ., Tokiwadai 79-5, Hodogaya, Yokohama, Kanagawa, Japan, kishi-sota-mx@ynu.jp
[2]Faculty of Eng., Yokohama National Univ., Tokiwadai 79-5, Hodogaka, Yokohama, Kanagawa, Japan, taraki@ynu.ac.jp
e-mail: kishi-sota-mx@ynu.jp

**Keywords:** PEFC, cold start, condensed water, frozen water, supercooled water, ice bridge

## INTRODUCTION

When a polymer electrolyte fuel cell (PEFC) is operated below the sub-zero temperature, the generated water remains inside PEFC as super-cooled water or ice [1]. Freezing water interfere with the the supplied reactive gas and it will cause shutdown of PEFC operation [2]. Therefore, understanding the mechanism of water freezing is necessary for achieving high performance of PEFC cold start. Many studies have been conducted on freezing about large sized droplets dropped with a pipette (1~100 µl) and condensation frosting. In the phenomenon of condensation frosting, during the initial stage of freezing propagation, what is called ice bridges, in which ice grows like a bridge from ice to adjacent supercooled droplets, has been identified. This is thought to be caused by condensation of vapor supplied from the supercooled droplets to the ice due to the difference in saturated vapor pressure between the ice and the supercooled droplets [3]. In this study, we treated the surfaces with hydrophobic and hydrophilic patterns using photolithography to obtain droplets with controlled spacing and size, and experiments were conducted to visualize freezing at the droplet size scale that occurs in PEFC.

## METHODS

Figure 1 shows a schematic diagram of the observation area. To control the shape of the liquid water condensing on the sample substrate, the silicon wafer surface was treated with hydrophilic and hydrophobic patterns. The diameter of the hydrophilic circle is $D$ [µm] and the distance between the circles is $G$ [µm]. Figure 2 shows the pattern shape and Table 1 shows the pattern dimensions. The experimental process was conducted in two steps. First, the cooling plate was cooled to 0 °C, and humidity controlled air with super-saturation ration 2 and the dew point 9.9 °C was supplied to the surface for a certain time. Condensate droplets were mainly generated to hydrophilic areas. Second, supplying gas was stopped and the temperature of the cooling plate was set to -14 °C to freeze the droplets on the surface.

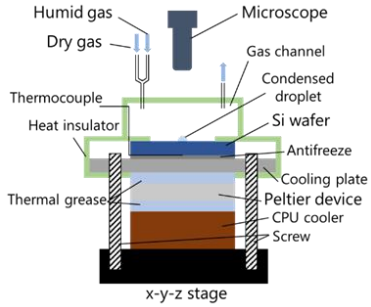


Fig. 1 Schematic of observation surface and around.

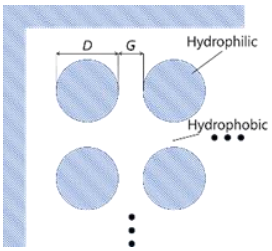


Fig. 2 Pattern geometry.

Table 1 Pattern dimensions.

| Diameter | Gap |
|---|---|
| *D* [μm] | *G* [μm] |
| 60.0 | 15.0 |
| 80.0 | 20.0 |

## RESULTS AND DISCUSSION

Freezing propagation was observed in the experiments, and the propagation was caused by ice bridge growth. Therefore, we measured local ice bridge growth velocity. The measurements of the difference in the gap and ice bridge length over time are shown in Fig. 3. The growth velocity increased as ice bridge approached the supercooled droplets and the measurements are similar to the local one-dimensional water vapor diffusion model.

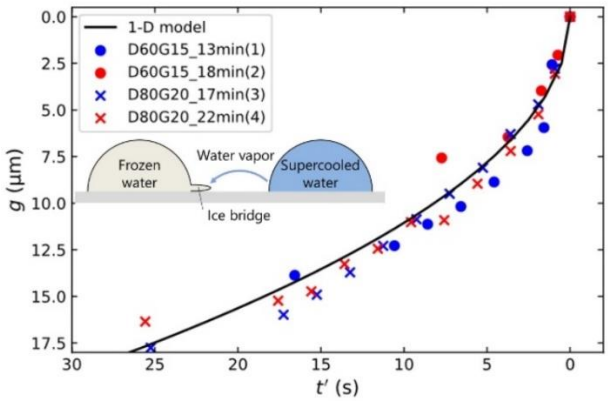


Fig. 3 Ice bridge growth over time

## CONCLUSION

Microscale droplets freezing was observed on wetting-patterned surfaces, and freezing propagation called ice bridge was visualized and measured.

## REFERENCES

[1] Y. Ishikawa et al., Super-cooled water behavior inside polymer electrolyte fuel cell cross-section below freezing temperature Journal of Power Sources, 179 (2008) 547-552.

[2] Y. Otsuki et al., Measurement of solidification heat from supercooled water freezing during PEFC cold start and visualization of ice distribution, Int. J. Hydrog. Energy 45 (31) (2020) 15600-15610.

[3] N. Nath et al., On Localized Vapor Pressure Gradients Governing Condensation and Frost Phenomena, Langmuir, 32 (2016) 8350-8365.

# 11 THE EFFECT OF SUPPORT MATERIAL ON CARBON DEPOSITION ON OXYGEN CARRIERS FOR THE CHEMICAL LOOPING PROCESS

Özge Kiziltan[1], Michael Lammer[1,2], and Viktor Hacker[1]

[1]Working Group Fuel Cells and Hydrogen, Institute of Chemical Engineering and Environmental Technology Graz University of Technology, Inffeldgasse 25/C/EG, 8010 Graz, Austria,
[2]BEST - Bioenergy and Sustainable Technologies GmbH, Inffeldgasse 21b 8010 Graz Austria
e-mail: kiziltan@tugraz.at

**Keywords:** hydrogen production, chemical looping, oxygen carrier, carbon deposition

## INTRODUCTION

Hydrogen is a carbon-free secondary energy source that is produced in various pathways, majorly from fossil fuel sources [1]. Green hydrogen production methods need to be established and utilized for total decarbonization. The chemical looping technology is a promising solution for carbon-free hydrogen production. The technology utilizes oxygen carriers to cyclically be reduced by syngas and be reduced by steam to produce hydrogen. Iron oxide is a commonly used oxygen carrier for its high redox activity, vast availability, and low environmental impact [2]. Due to its low resistance to sintering, high melting metal oxide material is commonly used on iron-based oxygen carriers [3]. One of the major issues for the chemical looping process is the solid carbon formation during operation due to lower temperatures in the system during heat-up and cool-down steps. Solid carbon formations compromise the purity of the produced hydrogen stream as they have the potential to be oxidized in the steam oxidation step and generate carbonaceous content.
The aim of this study is to gain a deeper understanding on carbonaceous gas generation during the chemical looping for hydrogen production process. The effect of the support materials, namely $TiO_2$, $Al_2O_3$ and $MgAl_2O_4$ on carbon deposition and carbon oxidation is tested on built reactor system in the temperature range of 800-300 ºC. The composition of the outlet stream is continuously measured by optical gas analysers. Additionally ex-situ characterization methods such as XRD, EDX and SEM are utilized to analyse the changes in the morphology, crystallinity, composition and the porosity.
Iron based oxygen carriers on the respective support materials were synthesized by the mechanical mixing and the solution combustion methods. In order to observe the maximum influence of the support material, the $Fe_2O_3$:support weight ratio of the oxygen carriers were set to be 60:40. Instead of the syngas, carbon monoxide was used as a fuel to enhance potential deposition. Synthetic air is used as an oxidizer to fully oxidize the deposited carbon. For each temperature point, one cycle of reduction and one cycle of oxidation were conducted. The system was purged with nitrogen in each step. A carbon balance for each temperature step is conducted via the data generated from the gas analyser. The results show that, the impact of the support material alone is negligible. All the samples exhibit deposition in intermediate temperatures. Contrary to the theoretical data, the deposition was observed to be negligible in the lower temperature range. According to the XRD measurements, most of the deposition has occurred on the surface of the oxygen carriers. Scanning electron microscopy showed a sheet like formation on the surface of the bulk, which is interpreted as the migrated of Fe atoms to the surface of the bulk for each sample. XRD measurements on the sample proved the migration of the Fe to the surface as a concentration gradient is observed. Fe is

known to catalyse carbon deposition, which explains the formation of solid carbon being concentrated on the surface. The oxygen carrier supported on $Al_2O_3$ and $MgAl_2O_4$ showed similar results in terms of the activity and carbon deposition whereas the oxygen carrier supported on $TiO_2$ showed the least amount of deposition as well as redox activity. Further research is necessary to further understand the relationship between the redox activity and the carbon deposition.

REFERENCES


[1] F. Qureshi, M. Yusuf, M. A. Khan, et al., “A state-of-the-art review on the latest trends in hydrogen production, storage, and transportation techniques,” Fuel, vol. 340, p. 127 574, 2023

[2] L. Protasova and F. Snijkers, “Recent developments in oxygen carrier materials for hydrogen production via chemical looping processes,”Fuel, vol. 181, pp. 75–93, 2016

[3] Y. De Vos, M. Jacobs, I. Van Driessche, P. Van Der Voort, F. Snijkers, and A. Verberckmoes, “Processing and characterization of fe-based oxygen carriers for chemical looping for hydrogen production,” International Journal of Greenhouse Gas Control, vol. 70, pp. 12–21, 2018

# 12 TOWARDS A FACILE SYNTHESIS METHOD OF IRON-BASED PLATINUM- FREE ELECTROCATALYST FOR POLYMER ELECTROLYTE FUEL CELLS

Winnie Kong[1], Emre Burak Boz[2], Antoni Forner-Cuenca[3]

[1]Eindhoven University of Technology, 5600 MB Eindhoven, Netherlands, w.y.kong@tue.nl
[2]Eindhoven University of Technology, 5600 MB Eindhoven, Netherlands, e.b.boz@tue.nl
[3]Eindhoven University of Technology, 5600 MB Eindhoven, Netherlands, a.forner-cuenca@tue.nl
e-mail: w.y.kong@tue.nl

**Keywords:** ORR catalyst, platinum-free, zeolite

The transportation sector, mainly powered by fossil fuels, is responsible for approximately 14% of all greenhouse gas emissions [1]. Polymer electrolyte fuel cells (PEFCs) are promising candidates for sustainable transport as they only emit water, can be refilled fast, and enable long ranges with a single refill of hydrogen. However, their current costs and dependence on scarce materials challenge their broad implementation in heavy-duty and maritime transportation [2]. Another challenge is catalyst degradation (by dissolution, corrosion, agglomeration or detachment) during operation limiting the application of PEFCs for heavy-duty and maritime transport where long lifetime hours of over 35000 hours are desired [3]. The state-of-the-art catalyst layers are based on platinum nanoparticles supported on carbon, and global efforts have been made to develop high-activity catalysts with reduced platinum contents, including platinum alloys such as Pt-Ni [4] and Pt-Co [5]. While platinum-based materials remain the most active for the oxygen reduction reaction, their high cost and low durability during operation motivate the exploration of alternative materials.
Platinum group metal-free catalysts have gained prominence for PEFCs, where Fe-N-C based catalysts have shown high oxygen reduction reaction activity in acidic media [6], approaching that of platinum-based catalyst layers, yet their practical application is hindered by insufficient stability under operating conditions [7]. Inspired by recent efforts [6,7], our goal is to develop stable, active, and low-cost catalyst layers using earth-abundant materials. In this poster presentation, I will discuss my efforts to synthesize Fe-N-C catalysts by the incorporation of iron in a calcined zeolitic imidazolate framework. Post-treatments, such as acid-leaching and the utilization of secondary nitrogen precursors, are applied to activate the catalyst where efforts are made to develop non-hazardous approaches. Microscopic, spectroscopic and electrochemical techniques, such as the rotating disc electrode, are employed to correlate the catalyst composition with electrochemical performance. With this work, we hope to understand structure-performance relationships to enhance the performance of iron-based platinum-free catalysts for PEFCs.

ACKNOWLEDGEMENTS

SH2IPDRIVE has received funding from the Ministry of Economic Affairs and Climate Policy, RDM regulation, carried out by the Netherlands Enterprise Agency

REFERENCES


[1] Lamb, W.F., Wiedmann, T., Pongratz, J., Andrew, R., Crippa, M., Olivier, J.G., Wiedenhofer, D., Mattioli, G., Al Khourdajie, A., House, J. and Pachauri, SEnvironmental research letters, 16(7) (2021), p.073005.

[2] Thompson, S.T., Wilson, A.R., Zelenay, P., Myers, D.J., More, K.L., Neyerlin, K.C. and Papageorgopoulos, D. ElectroCat: DOE's approach to PGM-free catalyst and electrode R&D. Solid State Ionics, 319 (2018), pp.68-76.

[3] Cullen, D.A., Neyerlin, K.C., Ahluwalia, R.K., Mukundan, R., More, K.L., Borup, R.L., Weber, A.Z., Myers, D.J. and Kusoglu, A. New roads and challenges for fuel cells in heavy-duty transportation. Nature energy, 6(5) (2021), pp.462-474.

[4] Choi, S.I., Xie, S., Shao, M., Odell, J.H., Lu, N., Peng, H.C., Protsailo, L., Guerrero, S., Park, J., Xia, X. and Wang, J. . Synthesis and characterization of 9 nm Pt–Ni octahedra with a record high activity of 3.3 A/mgPt for the oxygen reduction reaction. Nano letters, 13(7) (2013), pp.3420-3425.

[5] Kumar, P.R., Suryawanshi, P.L., Gumfekar, S.P., Bhanvase, B.A. and Sonawane, S., 2018. Sonochemical synthesis of Pt-Co/C electrocatalyst for PEM fuel cell applications. Surfaces and Interfaces, 12 (2018), pp.116-123.

[6] Mehmood, A., Gong, M., Jaouen, F., Roy, A., Zitolo, A., Khan, A., Sougrati, M.T., Primbs, M., Bonastre, A.M., Fongalland, D. and Drazic, G. . High loading of single atomic iron sites in Fe–NC oxygen reduction catalysts for proton exchange membrane fuel cells. Nature Catalysis, 5(4) (2022), pp.311-323.

[7] Wan, X. and Shui, J. . Exploring durable single-atom catalysts for proton exchange membrane fuel cells. ACS Energy Letters, 7(5) (2022), pp.1696-1705.

# 13 EFFECT OF HYDROPHILIC CONTROL OF THE CATHODE ON PERFORMANCE OF THE TOLUENE DIRECT-HYDROGENATION ELECTROLYZER

Daiki Kudo,[2] Yoshiyuki Kuroda,[1.2] and Shigenori Mitsushima[1.2]

[1]Graduate School of Engineering Science, Yokohama National University, 79-5 Tokiwadai, Hodogaya-ku, Yokohama 240-8501, Japan
[2]Institute of Advanced Sciences, Yokohama National University, 79-5 Tokiwadai, Hodogaya-ku, Yokohama 240-8501, Japan
e-mail: ynugr-cel@ynu.ac.jp

**Keywords:** organic chemical hydride, membrane electrolysis, microporous layer

## INTRODUCTION

Introduction of renewable energy is expected to reduce carbon dioxide emissions. However, imbalance between the renewable energy supply and demand in regional and temporal is significant issue, and a system is required to store and transport electricity to convert into chemical energy like hydrogen. The toluene (TL)-methylcyclohexane (MCH) of chemical hydride system is one candidate for a hydrogen energy carrier. The advantage of this system is that the TL-MCH is liquid at ambient temperature and pressure and uses conventional petroleum infrastructure. We focus on direct electrolytic hydrogenation TL with water decomposition using proton exchange membranes (PEM) to improve MCH synthesis with two-step process of hydrogen production by water electrolysis and chemical hydrogenation of TL. In this system, water decomposes to oxygen and proton at the anode, the proton transports through the PEM, and TL hydrogenates to MCH with the proton at the cathode. Here, there is an issue that the electroosmotic drag water of proton through the PEM inhibits TL transportation and electrohydrogenation [1].
In this study, the hydrophobicity control of cathode to improve Faraday efficiency has been investigated by enhancing water discharge from the cathode catalyst layer (CL) to improve TL mass transfer. In the cathode, We focused on the effect of the hydrophobicity of the microporous layer (MPL), which is between the CL and the carbon paper that works as backing of the CL and TL flow filed, on the performance of the electrolyzer by adding hydrophilic diatomite on the Faraday efficiency.

## EXPERIMENTAL

The anode was DSE® for oxygen evolution (De Nora Permelec Co., Ltd.), and the PEM was Nafion117® (DuPont). The cathode was three-layer structure of CL/microporous layer (MPL)/porous carbon substrate. Mixture of Ketjen black (EC-300J, LION), a diatomite (157607, MP Biomedicals) and a PTFE dispersion (31-JR, Mitsui DuPont Fluorochemicals) was coated onto carbon paper (TGP-H-090H, Toray) to form the MPL on the carbon substrate. Weight ratio of diatomite in MPL were 0, 4, 8, 12, and 16 wt%. PtRu/C (TEC61E54, TKK) catalyst mixed with 5 % Nafion® dispersion (DuPont) was coated on the MPL. The cathode electrode and PEM were hot-pressed at 120°C and 4 MPa for 3 min to make a membrane electrode assembly (MEA).
Cathode and anode reactants were 10 mL $min^{-1}$ circulation of 10% TL-MCH and 1mol $dm^{-3}$ $H_2SO_4$, respectively. Operation temperature was 60°C. The electrochemical measurements are chronoamperometry (CA), electrochemical impedance spectroscopy (EIS), and Faraday efficiency measurement. Faraday efficiency was determined with the volume ratio of generated hydrogen gas and toluene-methylcyclohexane solution obtained at the outlet of cathode chamber by Faraday's law.

## RESULT AND DISCUSSIONS

Figure 1 shows the internal resistance, the *IR*-corrected cell voltage and Faraday efficiency as a function of current density, respectively. The internal resistance was almost the same regardless of the diatomite addition. Therefore, the addition of the insulating diatomite in this range does not significantly increase the MPL resistivity. The addition of 8 wt% resulted in the lowest cell voltage and the highest Faraday efficiency. In addition, the cell voltage increased at the current density where the Faraday efficiency decreased. This would be due to the transition of the catalytic reaction from TL-hydrogenation to hydrogen generation.

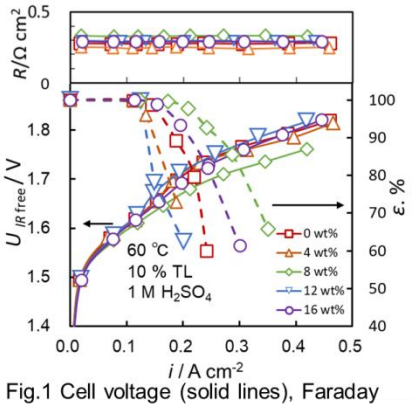


Fig.1 Cell voltage (solid lines), Faraday efficiency (dashed lines) and internal resistance as a function of current density with various weight ratio of diatomite

Figure 2 shows the EIS at 1.7 V with the various diatomite addition with an inset of the equivalent circuit with the resistances: $R_1$, $R_2$ and $R_3$, and constant phase elements: $CPE_2$ and $CPE_3$. They represent the internal resistance, cathodic and anodic charge transfer resistances with each parallel constant phase element, which corresponds to higher and lower frequency semi-circles, respectively. The assignment of the equivalent circuit is based on the experiments with various operation conditions in our previous study[2]. The $R_3$ was almost the same for various diatomite addition and the analysis of $R_2$ corresponds to mass transfer in the cathode catalyst layer.

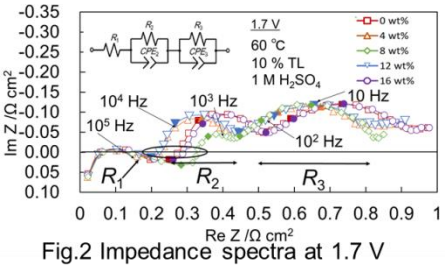


Fig.2 Impedance spectra at 1.7 V with various weight ratio of diatomite

Figure 3 shows the current density at 90% of Faraday efficiency and the $R_2$ of the cathodic charge transfer resistance at 1.7 V as a function of weigh ratio of diatomite in the MPL. The addition of 8 wt% resulted in the highest current density at 90% of Faraday efficiency and the lowest cathodic charge transfer resistance. The reduction in cathodic charge transfer resistance indicating that Improved TL mass transfer by hydrophilic diatomite becoming an outlet path for water. This improved Faraday efficiency.

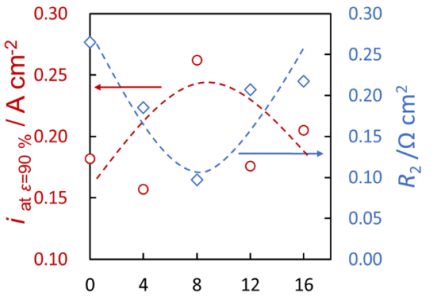


Fig.3 Current density at ε=90% (left side) and Cathodic reaction resistance at 1.7V (right side) as a function of weight ratio of diatomite

## ACKNOWLEGEMENTS

This work was based on results obtained from the Development of Fundamental Technology for Advancement of Water Electrolysis Hydrogen Production in Advancement of Hydrogen Technologies and Utilization Project (JPNP14021) commissioned by the New Energy and Industrial Technology Development Organization (NEDO). The anode was supplied by De Nora Permelec Ltd. We appreciate the person concerned them.

## REFERENCES

[1] K. Nagasawa, K. Tanimoto, J. Koike, K. Ikegami, S. Mitsushima, J. Power Sources, 439, 227070 (2019).

[2] K. Nagasawa, A. Kato, Y. Nishiki, Y. Matsumura, M. Atobe, S. Mitsushima, Electrochimica Acta, 459-465, 246 (2017).

# 14 INDUCED HYDROGEN CROSSOVER ACCELERATED STRESS TEST FOR PEM WATER ELECTROLYSIS CELLS

Eveline Kuhnert[1], Mathias Heidinger[1], Viktor Hacker[1], and Merit Bodner[1]

[1]Institute of Chemical Engineering and Environmental Technology, Inffeldgasse 25c, Graz, Austria
e-mail: eveline.kuhnert@tugraz.at

Polymer electrolyte membrane water electrolysis (PEMWE) is considered a promising solution for decarbonizing industry and establishing a sustainable hydrogen infrastructure. The central components of a PEMWE cell are represented by the membrane electrode assembly (MEA), comprising a polymer electrolyte membrane (PEM) integrated with catalyst layers (CLs) and porous transport layers (PTLs) for diffusion transport of water- and gases. The Nafion-based PEM is the weakest element of this system, susceptible to both chemical and mechanical degradation. Chemical degradation of the membrane occurs when hydrogen peroxide forms due to the crossover of product gases ($H_2$ and $O_2$) [1].

In this work, membrane failure due to induced hydrogen crossover has been addressed in a membrane-focused accelerated stress test (AST). The AST was conducted on a test cell employing asymmetric $H_2O$ and gas supply in open circuit voltage (OCV) mode, at two different temperatures (60 °C and 80 °C). Electrochemical characterization was performed at the beginning- and end of the testing period, revealing a 1.6-fold higher increase in high-frequency resistance (HFR) at 80 °C. The extent of hydrogen crossover was measured using a micro-GC, while the fluoride emission rate (FER) as indicator for membrane degradation was continuously monitored during the ASTs [1]. A direct correlation between FER and $H_2$ crossover was established, confirming accelerated membrane degradation at higher temperatures.

This research is performed under the HyGen project (K-Project HyTechonomy, FFG grant number 882510) which is supported by the Austrian Research Promotion Agency (FFG).

REFERENCES

[1] Kuhnert, E., Hacker, V. & Bodner, M. A Review of Accelerated Stress Tests for Enhancing MEA Durability in PEM Water Electrolysis Cells. International Journal of Energy Research 2023, 1–23 (2023).

[2] Kuhnert, E., Heidinger, M., Sandu, D., Hacker, V. & Bodner, M. Analysis of PEM Water Electrolyzer Failure Due to Induced Hydrogen Crossover in Catalyst-Coated PFSA Membranes. Membranes 13, 348 (2023).

# 15 IEA RESEARCH TECHNOLOGY COLLABORATION PROGRAMME ANNEX 31: POLYMER ELECTROLYTE FUEL CELLS

Michael Lammer[1,2], Merit Bodner[1], Bernhard Gollas[3], Brigitte Hammer[1], and Viktor Hacker[1]

[1]Graz University of Technology, Institute of Chemical Engineering and Environmental Technology, Inffeldgasse 25/C, 8010 Graz, Austria
[2]BEST - Bioenergy and Sustainable Technologies GmbH, Inffeldgasse 21b 8010 Graz Austria
[3]Graz University of Technology, Institute for Chemistry and Technology of Materials, Stremayrgasse 9, 8010 Graz, Austria
e-mail: michael.lammer@tugraz.at

**Keywords:** polymer electrolyte fuel cell, fuel conditioning, international cooperation, transfer of knowledge, IEA topical meeting, RSE-SEE

## INTRODUCTION

Within the framework of the research call in International Energy Agency *Annex 31: Polymer Electrolyte Fuel Cells*, international cooperation is being intensified at the Institute of Chemical Engineering and Environmental Technology and the Working Group for Fuel Cell Systems and Hydrogen Technology, Austria is being strengthened as a technology location and international networking is being promoted.
Within this Annex, fuel cell systems and associated components are characterised, reports and documentations are published and public relations are enhanced. The results are made available to national and international boards, the IEA, companies and institutions as well as the general public through dedicated websites and forums.

## PARTICIPATING COUNTRIES AND INTERNATIONAL EVENTS

Currently, 14 countries are operating within Annex 31 of the Technology Collaboration Programme on Advanced Fuel Cells: Austria, China, Denmark, Finland, France, Germany, Israel, Japan, Mexico, South Korea, Spain, Sweden, Switzerland and the USA (lead).


Fig.1: members of the conference hosting committee and the winner of the poster prize at RES-SEE 2022.

The topical meeting on *Potential for cost reduction and performance improvement of the IEA AFC TCP for PEMFC at component and system level* was held at TU Graz on 10 and 11 November 2021. On these two days, 11 presentations by researchers from academia and industry provided valuable insight into various topics ranging from component design over testing to economics.
The *8th Regional Symposium on Electrochemistry of South-East Europe* was held in Graz from 11 to 15 July 2022 (https://www.aseee.eu/index.php/rse-see-home). This forum has proven to be a place for fruitful debates, personal exchange and scientific discourse necessary for the further development of the field (Fig.1).

## RESEARCH ACTIVITIES AT TU GRAZ

The *GO DEFC* project is addressing the development of new low-cost anode and cathode catalysts with low precious metal content as well as new anion exchange membranes based on sustainable and low-cost materials for low-temperature fuel cells.
In the *HyStore* project, the focus is on hydrogen storage for cells, short stacks and entire fuel cell systems.
At the Institute of Chemical Engineering and Environmental Technology, the BioLOOP project focuses on the system integration of chemical looping processes for the utilisation of biomass. The proposed technology enables the regional use of biomass for hydrogen production in decentralised plants.
Within the framework of the FFG project *MILES* (Medium and Long Term Storage Technologies towards 100% renewable energy in Austria), a catalogue of criteria for storage systems is being developed in order to map them in a simulation model of the Austrian electricity system.
Efficient energy supply and storage from renewable raw materials are essential cornerstones for achieving the climate targets. The use of hydrogen as a secondary energy carrier is a suitable candidate for reducing greenhouse gas emissions in industry, energy and mobility. This is being specifically addressed and researched in the *ACCPETOR* project.

## ACKNOWLEDGEMENTS

Financial support by the Austrian Research Promotion Agency (FFG) through the Federal Ministry for Climate Action, Environment, Energy, Mobility, Innovation, and Technology (BMK) is gratefully acknowledged.

## REFERENCES

[1] IEA Technology Collaboration Programme, Advanced Fuel Cells, general information website. Obtainable online at: https://www.ieafuelcell.com/
[2] V. Hacker. Book of Abstracts: Topical Meeting on Potential for cost reduction and performance improvement of the IEA AFC TCP for PEMFC at component and system level, Austria, (2021).
[3] M. Lammer, K. Malli, R. Zacharias, A. Jany, K. Kocher, M. Grandi, B. Hammer and V. Hacker: Period report 2017-2019, IEA Fortschrittliche Brennstoffzellen (AFC) Annex 31: Polymerelektrolyt-membran-Brennstoffzellen, Austria, (2020).
[4] V. Hacker: Period report 2014-2017, IEA AFC Annex 31: Fortschrittliche Brennstoffzellen: Polymerelektrolytmembran-Brennstoffzellen, Austria, (2017).

# 16 DEVELOPMENT AND CHARACTERISATION OF GADOLINIUM DOPED CERIA THIN FILMS BY SPRAY PYROLYSIS FROM ENVIRONMENT-FRIENDLY PRECURSOR SOLUTIONS

Niklas Mayr[1], Stefan Edinger[2], T. Dimopoulos[3], and V. Subotic[4]

[1]AIT, Center for Energy; Giefinggasse 2, 1210 Vienna; niklas.mayr@ait.ac.at
[2]AIT, Center for Energy; Giefinggasse 2, 1210 Vienna; stefan.edinger@ait.ac.at
[3]AIT, Center for Energy; Giefinggasse 2, 1210 Vienna; theodoros.dimopoulos@ait.ac.at
[4]TU-Graz, IWT; Inffeldgasse 25/B, 8010 Graz; vanja.subotic@tugraz.at
e-mail: niklas.mayr@ait.ac.at

**Keywords:** SOFC, SOEC, GDC, material development, spray pyrolysis

## INTRODUCTION

A promising technology for the energy transition from fossil feedstocks like coal or oil to renewables, are solid oxide cells (SOC). An SOC can be both operated as a fuel cell and as an electrolyser. Thereby excess renewable electricity can be efficiently utilized to synthetise commodity chemicals such as hydrogen, ammonia, or synthetic gas. [1]

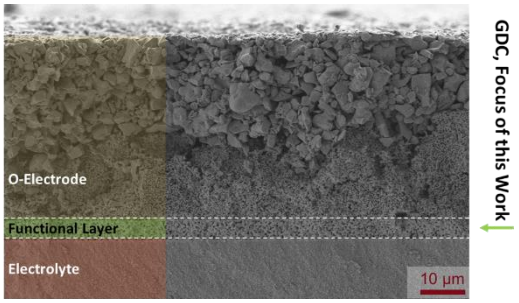


Figure 1: Cross-Section of the oxygen electrode of a commercial SOC.

However, to date, degradation and high cost prevent their large-scale application in industry. To tackle this, new modelling and monitoring approaches are developed [2], together with new materials and deposition methods. A versatile material deposition method for the development of reliable and cost-efficient SOCs, is ultrasonic spray pyrolysis (USP), using environmentally friendly precursors [3, 4]. In this work, the deposition by USP and characterisation of Gadolinium doped Ceria ($Ce_{0.2}Gd_{0.2}$-$O_3$, GDC) thin films, is discussed. An approximately 200 nm thick GDC diffusion barrier between the electrolyte and the $La_{0.6}Sr_{0.4}Co_{0.2}Fe_{0.8}$-$O_3$ (LSCF) oxygen electrode (see Figure 1) is an integral part of a SOC since the formation of undesired $La_2Zr_2O_7$ and $SrZrO_3$ phases in the interface is effectively prevented. [5]

## FILM DEPOSITION

GDC films are deposited with a Sono-Tek Exacta Coat® system, equipped with a Sono-Tek Impact® (120 kHz, 3.5 W) nozzle. 300 repetitions are conducted at a precursor flow rate of 0.5 ml min-1, a scan speed of 20 mm s-1, a shaping air pressure of 0.5 kPa and a temperature of 275 °C. The precursor is composed of 1/3 v% Ethanol and 2/3 v% diethylene glycol monobutyl ether and stoichiometric amounts of nitrate salts of Gadolinium and Cerium salts with a total metal concentration of 0.04 M. [5, 6] As substrates, indium-tin-oxide coated floating glass (ITO glass) and uncoated borosilicate glass (HT glass) are used.

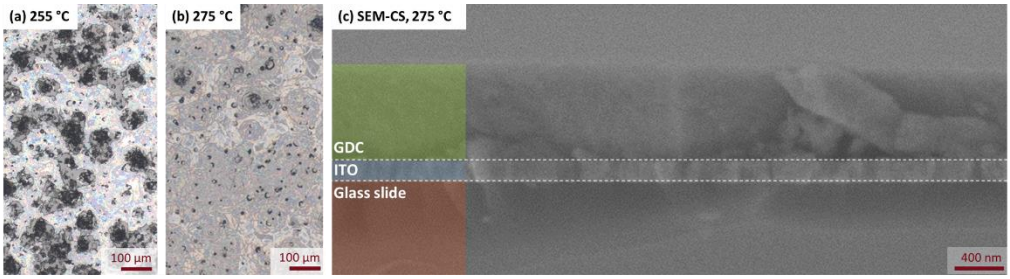

Figure 2: Representative light microscope images of depositions conducted at (a) 255 °C and (b) 275 °C. (c) cross-section of the deposition conducted at 275 °C.

FILM CHARACERISATION

After the deposition, the samples are first investigated with a light microscope (HORIBA XploRA PLUS). In Figure (a), a deposition conducted at a lower temperature of 255 °C is displayed. Large scale artefacts in the range of 100 µm and film defects are present. By contrast, as displayed in Figure (b), the artefacts are substantially less pronounced at a higher temperature of 275 °C. By investigating the cross section, displayed in Figure (c), with a SEM (Zeiss, Ultra 40), it is confirmed that apart from of the µm-scale artefacts an approximately 400 nm thick film of GDC was deposited.

To check the crystal structure of the films, the samples were further investigated with an XRD system (Cu Kα λ = 1.5419 Å, Thermo Fisher Scientific). The diffractograms are presented in Figure : The blue line represents the bare HT glass while the green line represents the pattern of the GDC deposited on the HT glass. Further the red line represents the ITO glass while the orange line represents the GDC deposition on the ITO glass. Given the distinct peaks at ~28.5°, 47.5° and 56°, indicated by the grey dashed lines, it is concluded that the GDC is multicrystalline, according to the GDC reference [96-156-2992]. The additional peaks at ~21.5, 30.5°, 35.5°, 50.5° and 60.5 can be clearly attributed to the ITO coating. The ITO peaks are less pronounced after the GDC deposition due to the additional layer.

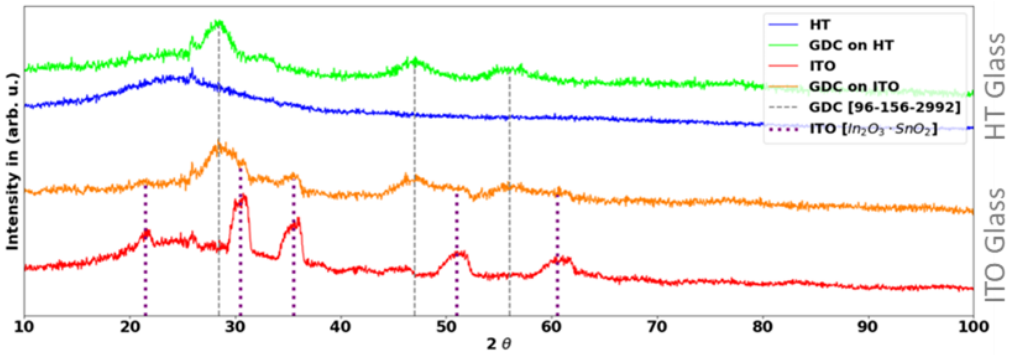

Figure 3: Representative XRD pattern with GDC (grey, dashed) and ITO pattern (purple, dotted line)

Finally large area depositions are investigated with the recently developed Inline Computational Imaging (ICI) Microscopy [7]: By acquiring images with a light microscope under four to six different illumination directions above a continuously moving sample, the morphology is calculated as displayed in Figure . Since the scan rate (3 mm3 s-1) is substantially faster compared to the other methods, a whole cell can be scanned without destructing the sample. Thereby defects can be efficiently identified and consequently more closely investigated.

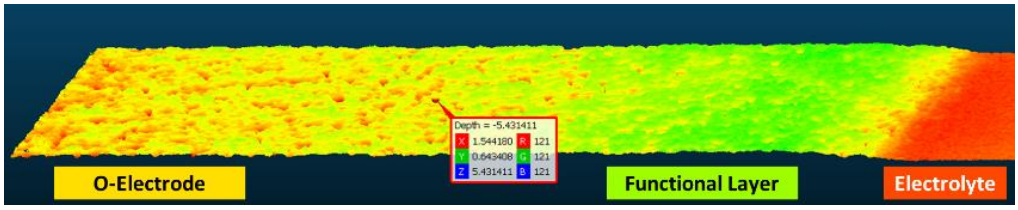

Figure 4: Surface of the rim where the individual layers of a commercial SOC (see Figure ) are exposed.

## CONCLUSION & OUTLOOK

In the present work a recipe for the efficient deposition of GDC thin films with a solvent system proposed for the ultrasonic spray deposition of LSCF [6] was developed. Thereby both films could be deposited with the same solvents. Further, toxic solvents like ethylene glycol are omitted. Next steps are to investigate water-based precursors systems and depositions of the perovskite LSCF electrode. Finally electrochemical measurements need to be performed to determine the performance of the manufactured cells.

## REFERENCES

[1] Ni, Meng, Michael KH Leung, and Dennis YC Leung. "Technological development of hydrogen production by solid oxide electrolyzer cell (SOEC)." International journal of hydrogen energy 33.9 (2008): 2337-2354.

[2] Mütter, Felix, et al. "Artificial intelligence for solid oxide fuel cells: Combining automated high accuracy artificial neural network model generation and genetic algorithm for time-efficient performance prediction and optimization." Energy Conversion and Management 291 (2023): 117263.

[3] Edinger, S., Bansal, N., Bauch, M., Wibowo, R. A., Újvári, G., Hamid, R., ... & Dimopoulos, T. (2017). Highly transparent and conductive indium-doped zinc oxide films deposited at low substrate temperature by spray pyrolysis from water-based solutions. Journal of Materials Science, 52, 8591-8602.

[4] Wolf, M., Madsen, G. K., & Dimopoulos, T. (2023). Accelerated screening of Cu–Ga–Fe oxide semiconductors by combinatorial spray deposition and high-throughput analysis. Materials Advances.

[5] Szymczewska, D., Karczewski, J., Chrzan, A., & Jasinski, P. (2017). CGO as a barrier layer between LSCF electrodes and YSZ electrolyte fabricated by spray pyrolysis for solid oxide fuel cells. Solid State Ionics, 302, 113-117.

[6] Beckel, D., Dubach, A., Studart, A. R., & Gauckler, L. J. (2006). Spray pyrolysis of La 0.6 Sr 0.4 Co 0.2 Fe 0.8 O 3-δ thin film cathodes. Journal of electroceramics, 16, 221-228.

[7] Stolc, S., Thanner, P., & Clabian, M. (2018). Inline Computational Imaging: single sensor technology for simultaneous 2D and 3D high definition inline inspection. Imaging and Machine Vision Europe, (89), 34-35.

# 17 COOLING SYSTEMS ON PEM FUEL CELL

Abdelhakim Merdjani[1]

[1]Warsaw University of Technology, Poland,
e-mail: abdelhakim.merdjani.dokt@pw.edu.pl

**Keywords:** PEMFC, cooling system, CFD

## INTRODUCTION

Nowadays proton exchange membrane fuel cell (PEMFC) one of efficient energy systems and have potential to compensate our energy needs in the near future for many industrial sectors, their efficiency depends on performance optimization of each component like the membrane which is the main component is this system, PEMFC inevitably emit a certain amount of heat while generating electricity, due chemical reaction the temperature of membrane increases during operation which is between 60 °C to 120 °C, this increment can decrease the cell performance.

## METHOD

During the operation of PEMFCs, various electrochemical reactions take place, resulting in the generation of heat. Effective cooling is crucial to maintain optimal operating temperatures within the fuel cell, as excessive heat can lead to performance degradation, reduced efficiency, and even cell failure. Cooling systems in PEMFCs are responsible for dissipating the generated heat and maintaining the desired temperature range for proper operation. The cooling system ensures uniform temperature distribution across the fuel cell stack and prevents localized hotspots that could negatively impact cell performance and durability.
Different methods have been used in the thermal management of fuel cells. Cooling with cathode airflow is only used with small-size fuel cells. In this case, the outside area of the stack must be larger than the active area for the stack, and heat is dissipated from the outside area by convection. The disadvantage of this cooling method is that it requires larger cathode channels, which increases the stack's size. In fuel cells larger than 100 W, air needs to be forced through separate cooling channels. In some cooling designs, heat is released from the stack to the surroundings by highly conductive heat spreaders placed adjacent to the air channels [1]. Cooling with liquids (e.g., antifreeze, water) is used because liquids have higher specific heats and thermal conductivities than air. This kind of cooling is used frequently in the automotive industry (figure 1).

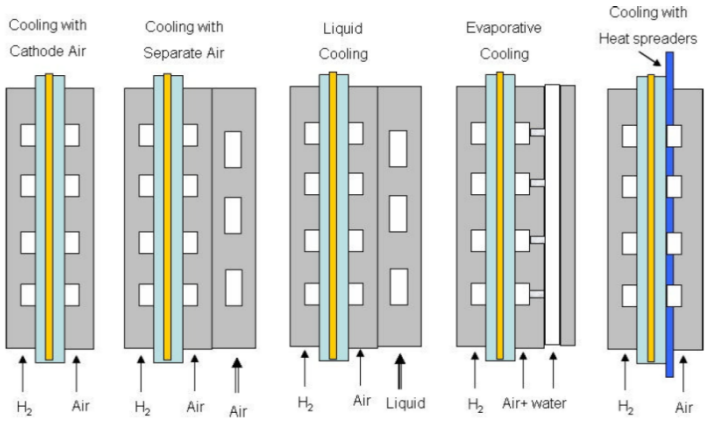


Figure 1. System configurations

The simulation setup and definition of the 3D model (figure 2) of a Proton Exchange Membrane Fuel Cell (PEMFC) with a cooling system was conducted using ANSYS software. The simulation aims to analyze the thermal and fluid dynamics behavior of the PEMFC, considering the cooling system's impact on performance and temperature distribution within the fuel cell.

The proposed cooling system is water channels (3 channels for each anode and cathode) with a velocity of 1m/s.

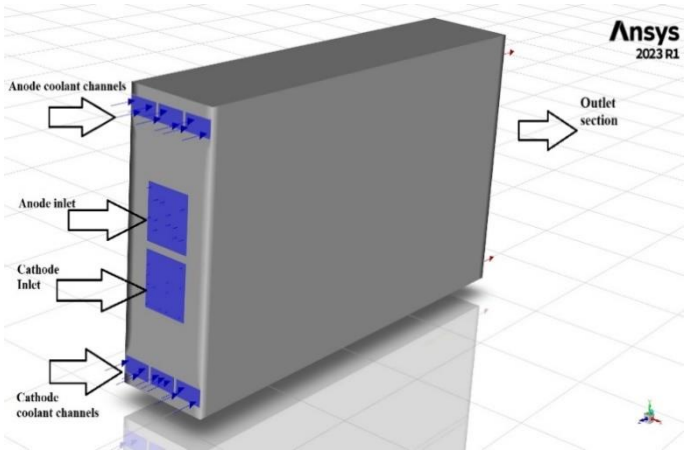


Figure 2. 3D PEMFC model

RESULTS

The polarization curve is a crucial index for assessing proton exchange membrane fuel cell performance, the polarization curves of the straight flow field channel with and without cooling channels shown in figure 3. The performance of FC with cooling channels is better as shown, the current density of the cell with cooling channels is 0.54 A/cm2 when the voltage is 0.7 Which is 35% higher and 2.03 A/cm2 when the voltage is 0.3 V which is 27% greater than no-cooling cell.

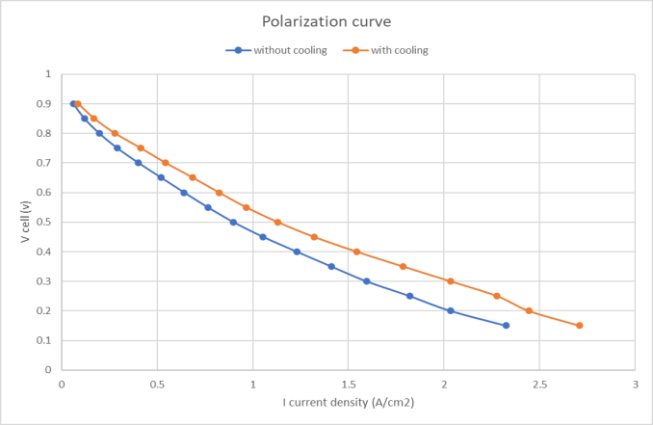


Figure 3. Polarization curve

# 18 DESIGN OF SELF-REPAIRING SUPPOTED ANODE CATALYSTS FOR ALKALINE WATER ELECTROLYSIS WITH BOTH OER ACTIVITY AND DURABILITY VIA COLLOIDAL SELF-ASSEMBLY

Daiji Mizukoshi,[1] Tatsuya Taniguchi,[2] Yuta Sasaki,[2] Yoshinori Nishiki,[3] Zaenal Awaludin,[3] Takaaki Nakai,[3] Akihiro Kato,[3] Shigenori Mitsushima,[1,4] Yoshiyuki Kuroda[1,4]

[1]Grad. School of Eng. Sci., Yokohama Natl. Univ., 79-5 Tokiwadai, Hodogaya-ku, Yokohama 240-8501, Japan
[2]Kawasaki Heavy Ind., Ltd., 1-1 Kawasakicho, Akashi, Hyogo, 673-8666, Japan
[3]De Nora Permelec, Ltd., 2023-15 Endo, Fujisawa, Kanagawa, 252-0816, Japan
[4]Adv. Chem. Energy Res. Center, Inst. of Adv. Sci., Yokohama Natl. Univ., 79-5 Tokiwadai, Hodogaya-ku, Yokohama 240-8501, Japan
e-mail: ynugr-cel@ynu.ac.jp

**Keywords:**. alkaline water electrolysis, renewable energy, self-repairing catalyst, supported catalyst, OER activity, durability.

## INTRODUCTION

When an alkaline water electrolyzer is powered by renewable energy, electrodes degrade due to reverse current generated on shutdown.[1] We have reported self-repairing catalysts based on hybrid cobalt hydroxide nanosheets (Co-ns), and β-FeOOH nanorods (Fe-nr).[2,3] Our previous studies showed that Co-ns formed thick catalyst layer with highly conductive framework, whereas Fe-nr formed a thin layer with much higher OER activity than that of Co-ns. These features can be used to design self-repairing supported catalysts with Fe-nr acting as the active site and Co-ns as the support. Here, we demonstrate the design of self-repairing supported catalysts, consisting of both Co-ns and Fe-nr. Co-ns promotes stacking of the catalysts on the electrode, and Fe-nr forms active sites.

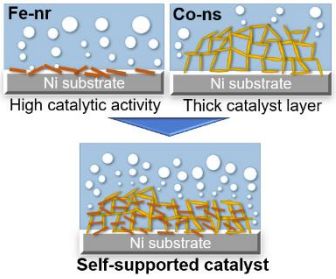


Fig. 1 Illustrations of the formation of the supported catalyst composed of Fe-nr and Co-ns.

## EXPERIMENTAL

Co-ns[2] and Fe-nr[3] were synthesized according to the literature. Electrochemical tests were performed in a 1.0 M KOH, using a PFA three-electrode cell. A nickel plate, a nickel coil, and a reversible hydrogen electrode were used as the working, counter, and reference electrodes, respectively. The Co-ns dispersion, Fe-nr dispersion, or their mixture (each concentration of catalyst weights is x ppm, y ppm, x + y = 80 ppm, respectively) was added in the electrolyte. Catalysts were deposited by repeating the following processes 10 times according to our previous report:[2] i) chronopotentiometry at 800 mA $cm^{-2}$ for 30 min, ii) cyclic voltammetry (CV) between 0.5 and 1.8 V vs. RHE at 5 mV $s^{-1}$, iii) CV between 0.5 and 1.6 V vs. RHE at 50 mV $s^{-1}$, and iv) electrochemical impedance spectroscopy at 1.6 V vs. RHE. Furthermore, an accelerated durability test (ADT) [4] was conducted 2000 cycles to examine the degradation.

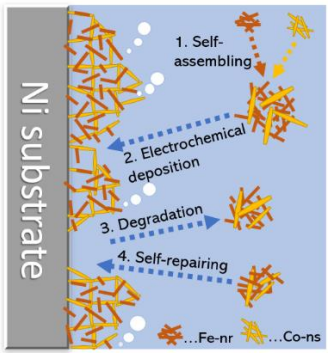


Fig. 2 Illustrations of self-repairing supported catalysts forming catalyst layer.

## RESULTS AND DISCUSSION

The synthesis of Co-ns and Fe-nr was confirmed by XRD, FTIR, TEM, and elemental analyses. Co-ns is modified with tripodal ligand, whereas Fe-nr is non-modified. The electrophoretic mobilities of Co-ns and Fe-nr were 1.98 and –2.80 μm cm $V^{-1}$ $s^{-1}$ at pH 9.7. Because Co-ns and Fe-nr are oppositely charged, they are expected to be self-assembled into a composite in the electrolyte.

The OER polarization curves during the repeated electrolysis are shown in the Fig. 3. The OER activity of the electrode prepared from the mixture of Co-ns and Fe-nr (the ratio of Fe-nr = 7.3%) was higher than those of the electrodes prepared from only one component. The OER overpotential at 100 mA $cm^{-2}$ (η100) of the composite catalyst was 291 mV after 300 min of electrolysis. The η100 of Co-ns and Fe-nr were 310 and 353 mV, respectively.

The mass of deposited Fe (MFe) and the overpotential at 100 mV as a function of the ratio of Fe-nr is shown in the Fig. 3. The MFe was 48.5 μg $cm^{-2}$ when the Fe-nr ratio was 7.3%, whereas it was 2.00 μg $cm^{-2}$ when only Fe-nr was used. MFe is correlated with the OER activity.

The results of ADT with the composite catalyst dispersed in the electrolyte to conduct self-repairing protocol (Fig. 5) shows that there was little degradation after 2000 cycles of start-up and shut-down. Therefore, these composite catalysts have excellent stability. However, when no composite catalyst was dispersed in the electrolyte, meaning that no self-repairing protocol was conducted, η100 gradually increased in the 2000 cycles (Fig. 6). The degradation behavior was milder than that of the Fe-nr only; thus, the composite catalyst exhibited the improved stability due to supporting on Co-ns.

In conclusion, co-deposition of Fe-nr and Co-ns produced new self-repairing composite catalysts with both high activity and high durability. This is the first report of self-repairing supported catalysts for alkaline water electrolysis powered by renewable energy.

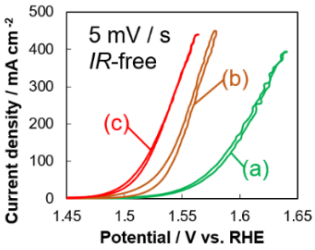


Fig. 3 OER polarization curves of (a) Co-ns, (b) Fe-nr, (c) the composite catalyst (7.3 % Fe-nr, 92.3 % Co-ns).

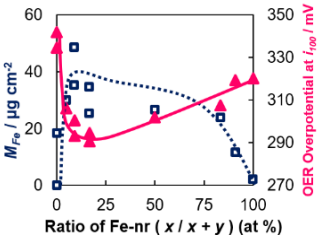


Fig. 4 The mass of deposited Fe ($M_{Fe}$) and the OER potential at 100mV as a function of the ratio of Fe-nr.

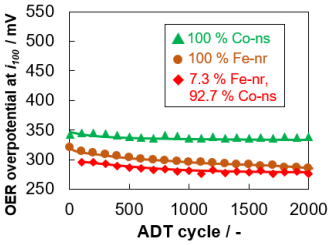


Fig. 5 OER potential at 100 mA $cm^{-2}$ as a function of the ADT cycle with self-repairing protocol.

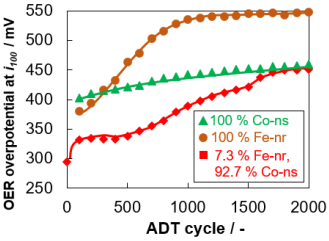


Fig. 6 OER potential at 100 mA $cm^{-2}$ as a function of the ADT cycle without self-repairing protocol.

ACKOWLEDGEMENTS

A part of this study was supported by KAKENHI (Grant-in-Aid for Scientific Research 20H02821) from Japan Society for the Promotion of Science (JSPS).

REFERENCES

[1] Y. Uchino et al., Electrocatalysis 9, 67 (2018).
[2] Y. Kuroda et al., Electrochim. Acta. 323, 1348122 (2019).
[3] Y. Kuroda et al., J. Sol-Gel Sci. Technol., 104, 647-658 (2022).
[4] A. Haleem et al., Electrochemistry. 89(2), 186 (2021). .

# 19 UNSTEADY POWER GENERATION CHARACTERISTICS OF PROTONIC CERAMIC FUEL CELL WHEN HUMIDIFICATION RATIO OF FUEL GAS IS SWITCHED

Takeru Murakami[1], Takuto Araki[2]

[1]Graduate School of Engineering Science, Yokohama National University,79-5 Tokiwadai, Hodogaya-ku, Yokohama 240-8501, Japan, murakami-takeru-hy@ynu.jp
[2]Faculty of Engineering, Yokohama National University, 79-5 Tokiwadai, Hodogaya-ku, Yokohama 240-8501, Japan, taraki@ynu.ac.jp
e-mail: murakami-takeru-hy@ynu.jp,

**Keywords:** PCFC, relaxation time, ohmic resistance

## INTRODUCTION

In recent years, there has been growing interest in developing protonic ceramic fuel cells (PCFCs) with proton conductive electrolyte. One of these reasons is that PCFCs have a possibility of higher generation efficiency than that of solid oxide fuel cells (SOFCs) with oxide-ion conductive electrolyte, due to less fuel dilution at fuel electrode side using $H_2$ fuel. The power generation characteristics of a PCFC depends on the humidification ratio of supply gas. It is very important to clarify how vapor affects the power generation, in order to optimize the operation.
We measured the transition of High Frequency Resistance (HFR) using the cells with varying electrolyte thickness to elucidate the transport characteristics inside electrolyte.

## EXPERIMENTAL

Measurement of HFR is performed by using PCFC cell adapting $BaZrO_3$-based perovskite as its electrolyte. We prepared cells with varying electrolyte thickness. The humidification ratio of supplied fuel gas is instantaneously switched between low and high humidity. The gas concentration on the air electrode (Air: 97%, $H_2O$: 3%) and the hydrogen concentration on the fuel electrode ($H_2$: 50%) remained fixed. The measurement device employed in this study was the Bio-Logic SP-150, manufactured by Bio-Logic.

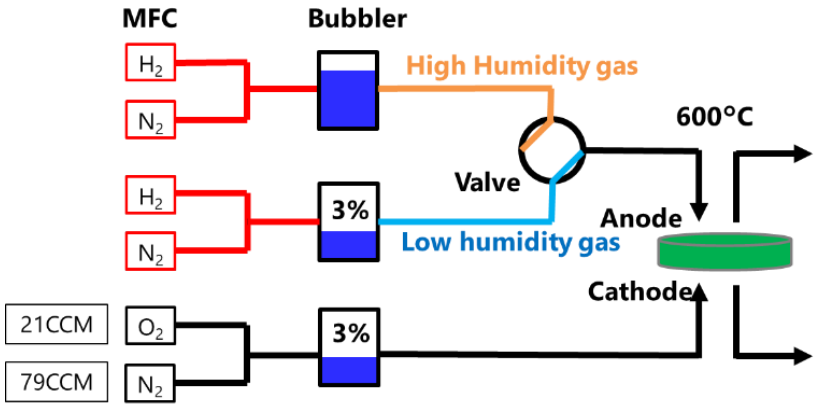


Fig.1 Schematic diagram of experiment system

## RESULTS AND DISCUSSION

Transition of HFR is shown in Fig.2. Fig. 2 presents the non-dimensionalized results of the HFR time transition for cells with different electrolyte membrane thicknesses, with each value normalized by its respective steady-state value. It was observed that increasing the electrolyte membrane thickness results in an increased response time constant. Numerical analysis and that result showed that the OH･O diffusion inside electrolyte mainly determines the relaxation time.

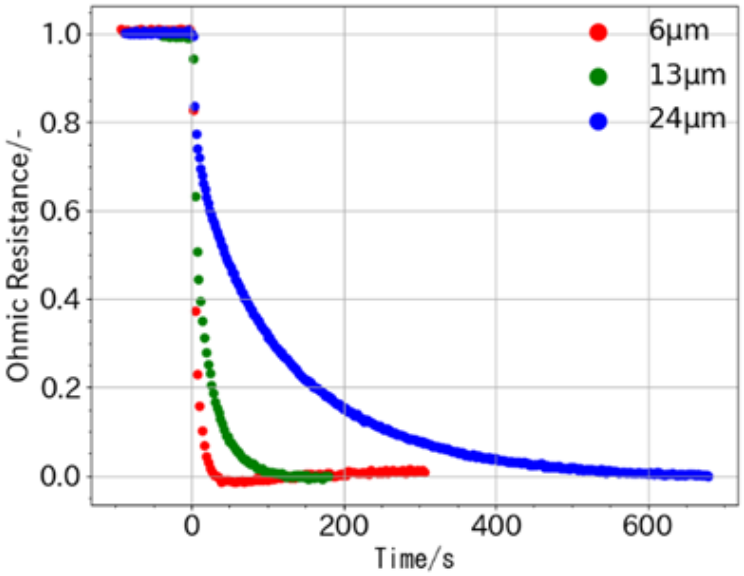


Fig.2 Transition of HFR when steam concentration is switched from 3% to 15%

## ACKNOWLEDGMENTS

Part of these results were obtained as a result of the New Energy and Industrial Technology Development Organization (NEDO) commissioned research and development of ultra-high efficiency proton-conducting ceramic fuel cell devices (JPNP20003).

# 20 EFFECT OF WATER VAPOR CONCENTRATION ON POWER GENERATION CHARACTERISTICS OF PROTONIC CERAMIC FUEL CELL

Yohei Nagata[1], Takuto Araki[2]

[1]Grad. Sch. Of Eng. Sci., Yokohama National Univ., Tokiwadai 79-5, Hodogaya, Yokohama, Kanagawa, Japan, nagata-yohei-tv@ynu.jp
[2]Faculty of Eng., Yokohama National Univ., Tokiwadai 79-5, Hodogaka, Yokohama, Kanagawa, Japan, taraki@ynu.ac.jp
e-mail: nagata-yohei-tv@ynu.jp

**Keywords:** SOFC, PCFC, proton conductivity, water vapor, fuel utilization

## INTRODUCTION

Protonic ceramic fuel cells (PCFCs) use $BaZrO_3$ ceramics with a perovskite structure as the electrolyte, which absorbs water vapor and thus exhibits proton conductivity [1]. In PCFC, the anode is generally used in a composite form of NiO and electrolyte materials for the following reasons: to increase the reaction field and improve the electrode performance, and to approximate the thermal expansion behavior of the electrolyte [2]. Therefore, in PCFCs, the proton conductivity of each electrode and electrolyte changes depending on the surrounding water vapor concentration, which affects the power generation performance [3]. Furthermore, in high fuel utilization operations, the hydrogen concentration decreases and the water vapor concentration increases toward the outlet of the gas channel due to hydrogen consumption. However, few studies have been reported on the effects of water vapor concentration in the anode gas of PCFCs on their power generation characteristics.. In this study, the relationship between the amount of water vapor in the feed gas and the power generation performance was investigated using a PCFC with a $BaZr_{0.8}Yb_{0.2}O_{3-\delta}$ electrolyte, which was selected because it does not produce reactants with NiO [4].

## EXPERIMENTAL

The coin-shaped cell with the compositions shown in Table 1 was used in the experiments. The compositions of hydrogen and water vapor in the gas supplied to the anode were varied as shown in Table 2, and the IV characteristics and electrochemical impedance at open circuit state and 0.85V were measured under each condition. The gas supplied to the cathode was fixed at O2 : 20% + $N_2$ : 77% + $H_2O$ : 3%, which is the same composition as air. The temperature in the cell holder was fixed at 600 °C.

Table 1. Details of evaluated cell

| | Materials | Thickness [mm] | Diameter [mm] |
|---|---|---|---|
| Cathode | LSCF ($La_{0.6}Sr_{0.4}Co_{0.2}Fe_{0.8}O_{3-\delta}$) | $3.0\times10^{-2}$ | 10 |
| Electrolyte | BZYb($BaZr_{0.8}Yb_{0.2}O_{3-\alpha}$) | $1.3\times10^{-2}$ | 20 |
| Anode | Ni-BZYb | $6.0\times10^{-1}$ | 20 |

Table 2. Conditions of anode gas

| Water vapor concentration [%] | Hydrogen concentration [%] |
|---|---|
| 3 | 97 |
| 20 | 80 |
| 40 | 60 |
| 60 | 40 |

RESULTS AND DISCUSSION

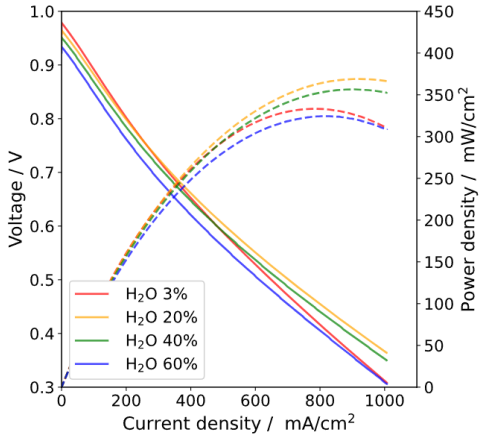


Fig. 1. I-V and power density curves on each anode water vapor concentration

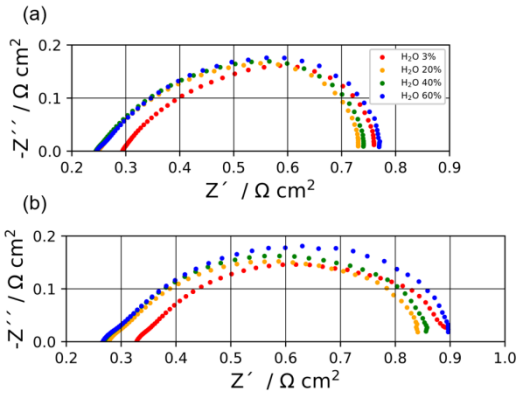


Fig. 2. Electrochemical impedance under (a) open circuit and (b) constant current on each water vapor concentration

The measured IV characteristics are shown in Fig.1. In Fig.1, the open circuit voltage decreases with increasing water vapor concentration due to the decrease in hydrogen concentration. The maximum power density on each condition shows that the power density increases from 3% to 20% of water vapor concentration, reaching a maximum value of 369 $mW/cm^2$ at 20%, while the power density decreases from 20% to 60% of water vapor concentration. The impedance measurements in Fig.2 show the decrease in ohmic resistance with increasing water vapor concentration, indicating the increase in the proton conductivity of the electrolyte. On the other hand, the polarization resistance increases with increasing water vapor concentration, presumably due to the decrease in hydrogen concentration and the increase in the concentration overpotential.

These results suggest that increasing the proton conductivity of the electrolyte from 3% to 20% of the water vapor concentration reduced the ohmic loss and improved the power density in Fig.1, while increasing the concentration overpotential between 20% and 60% of water vapor concentration worsened the power density.

REFERENCES

[1] Emiliana Fabbri, Daniele Pergolesi, and Enrico Traversa, Chem. Soc. Rev., 39(11), p. 4355-4369 (2010).

[2] Tomohiro Kuroha, Kosuke Yamauchi, Yuichi Mikami, Yoichiro Tsuji, Yoshiki Niina, Mizuki Shudo, Go Sakai, Naoki Matsunaga, and Yuji Okuyama, Int. J. Hydrog. Energy, 45(4), p. 3123-3131 (2020).

[3] Takaaki Somekawa, Yoshio Matsuzaki, Yuya Tachikawa, Hiroshige Matsumoto, Shunsuke Taniguchi, and Kazunari Sasaki, Int. J. Hydrog. Energy, 41(39), p. 17359-17547 (2016).

[4] Tomohiro Kuroha, Yoshiki Niina, Mizuki Shudo, Go Sakai, Naoki Matsunaga, Takehito Goto, Kosuke Yamauchi, Yuichi Mikami, and Yuji Okuyama, J. Power Sources, 506, 230134 (2021).

# 21 SEMI-HYDROGENATION SELECTIVITY ANALYSIS OF DIPHENYLACETYLENE ON PT1PD99/C CATALYST USING A PEM ELECTROLYZER

Hiroki Nakamura[1], Juri Harada[1], Naoki Shida[1], Kensaku Nagasawa[2], Yoshiyuki Kuroda[1], Mahito Atobe[1], Shigenori Mitsushima[1]

[1]Graduate school of Engineering Science, Yokohama National University, 79-5 Tokiwadai, Hodogaya-ku, Yokohama 240-8501, Japan
[2]Fukushima Renewable Energy Institute, National Institute of Advanced Industrial Science and Technology, 2-2-9 Machiikedai, Koriyama 963-0298, Japan
e-mail: ynugr-cel@ynu.ac.jp

**Keywords:** organic electrolysis, alkyne semi-hydrogenation, PEM electrolyzer, residual time, selectivity

## INTRODUCTION

Using renewable energy is crucial for achieving carbon neutrality, not only in energy production but also in organic synthesis. Traditionally, the widely employed Lindlar catalyst for stereoselective alkyne semi-hydrogenation has drawbacks such as toxic additives and reliance on hydrogen gas. Consequently, researchers have been exploring alternative approaches, one of which is electrolytic hydrogenation facilitated by a proton exchange membrane (PEM) electrolyzer. This method enables the selective synthesis of Z-alkenes under mild conditions, without toxic additives, by using renewable electricity and water as the hydrogen source instead of hydrogen gas. A previous study figured that the Pt1Pd99/C catalyst demonstrated high selectivity in forming cis-stilbene from diphenylacetylene (DPA) among various compositions of Pt-Pd/C catalyst. However, it lacked a comprehensive exploration of crucial factors for scaling up the PEM electrolyzer, such as flow field structure and electrolysis conditions, resulting in an insufficient evaluation of the Pt1Pd99/C catalyst for the application in a larger scale electrolyzer [1,2]. Therefore, our study aims to investigate the properties of the Pt1Pd99/C catalyst, including catalyst loading, reactant flow rate, potential, current density, and selectivity, to determine the appropriate electrolysis method in a practical, larger electrolyzer.

## EXPERIMENTAL

DSE® (De Nora Permelec) for the oxygen evolution and Nafion® 117 were used as the anode (DuPont) and the PEM, respectively. The cathode consisted of a 3.3 cm × 3.5 cm carbon paper (39BB, SGL) loaded with Pt1Pd99/C (ISHIFUKU Metal Industry Co., Ltd) ranging from 0.2 to 1.6 mgPtPd $cm^{-2}$. The cathode was hot-pressed onto the PEM at 120 °C and 6 MPa for 3 minutes to create a membrane cathode assembly. 1 M sulfuric acid circulated in the anode compartments, while a 1 M DPA cyclohexane solution flowed through the cathode compartments once. Electrochemical measurements included electrochemical impedance spectroscopy from 100 kHz to 0.1 Hz (10 mV amplitude), chronoamperometry from 1.3 to 2.0 V (catalyst loading dependency), and chronopotentiometry from 9 to 36 mA $cm^{-2}$ (flow rate and temperature dependency). Batch electrolysis with substrate solution circulation was conducted to enhance DPA conversion. HPLC quantified cis-stilbene and dibenzyl concentrations in electrolytes collected during the last 2 minutes of 5-minute electrolysis. Partial current values were obtained by multiplying concentrations, stoichiometric coefficients, Faraday's constant, and flow rate. Current efficiency represented the ratio of each partial

current to the total current. Selectivity was calculated as the ratio of cis-stilbene concentration to the combined product concentrations (cis-stilbene and dibenzyl), and conversion as the ratio of summed product concentration to the initial DPA concentration (1 M).

## RESULTS AND DISCUSSION

Figure 1 shows the current efficiencies of *cis*-stilbene and dibenzyl formation against the catalyst loading, at a flow rate of 1 mL $min^{-1}$, 60 °C and potentials of 0 and −0.2 V vs. RHE. The current efficiency of *cis*-stilbene formation increased, while that of dibenzyl formation decreased with decrease of catalyst loading. In particular, the catalyst loading dependency of the current efficiency for *cis*-stilbene and dibenzyl formation was significantly large at −0.2 V vs. RHE. Over-hydrogenation was suppressed with a low catalyst loading, that is, a thin catalyst layer, due to the short residual time in the catalyst layer.

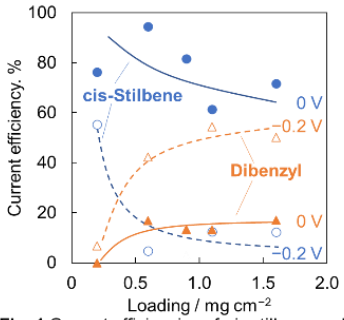


**Fig. 1** Current efficiencies of *cis*-stilbene and dibenzyl at 0 V (solid lines) and −0.2 V *vs.* RHE (dashed lines) versus the catalyst loading.

Figure 2 shows the current efficiencies of the products, cis-stilbene selectivity and DPA conversion as a function of DPA flow rates at the current density of 27 mA $cm^{-2}$ and 60 °C using 0.6 mg $cm^{-2}$ catalyst loaded electrode. The current efficiency and selectivity increased with frow rate. Hydrogen evolution dominated below 0.5 mL $min^{-1}$ of flow rate because the reactant supply to the catalyst layer was not sufficient. The flow rate increase improved the current efficiency and selectivity of cis-stilbene. Mass transfer between the catalyst layer and the flow channel enhanced at the higher flow rate, due to the fast product elimination from the reaction field, although the conversion decreased. Based on the data with once-through electrolysis, batch electrolysis, which is reactant circulated electrolysis, was designed. Low catalyst loading, higher than −0.2 V vs. RHE, high flow rate and high temperature suppresses over-hydrogenation to form dibenzyl and hydrogen evolution.

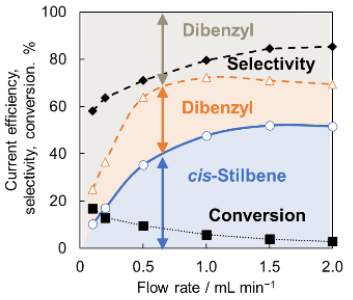


**Fig. 2** *cis*-Stilbene, dibenzyl, and other current efficiencies, selectivities using 0.6 mg $cm^{-2}$ catalyst-loaded electrode versus flow rate.

Figure 3 shows composition of substrate solution as a function of time. The conversion achieved approx. 40% with approx. 90% selectivity with 0.2 mg $cm^{-2}$ catalyst loading, at the flow rate of 2 mL $min^{-1}$, and at 18 mA $cm^{-2}$ where the potential is around −0.1 V vs. RHE. Nevertheless, for much higher conversion, another catalyst development is required to suppress the over-hydrogenation to form dibenzyl.

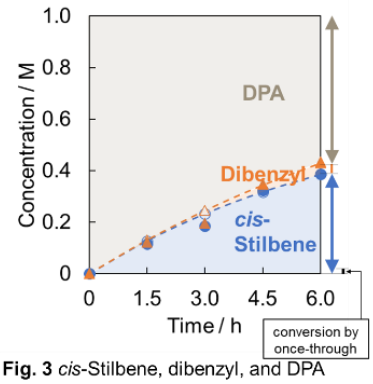


**Fig. 3** *cis*-Stilbene, dibenzyl, and DPA concentration change versus electrolysis time with a batch electrolysis.

ACKNOWLEDGEMENT

This work was financially supported by CREST (JST Grant 18070940). The authors are grateful to ISHIFUKU Metal Industry Co., Ltd. for providing the cathode catalysts.

REFERENCES

[1] S. Nogami, K. Nagasawa, A. Fukazawa, K. Tanaka, S. Mitsushima, M. Atobe, J. Electrochem. Soc., 167, 155506 (2020).

[2] S. Nogami, N. Shida, S. Iguchi, K. Nagasawa, H. Inoue, I. Yamanaka, S. Mitsushima, M. Atobe, ACS Catal., 12, 5430 (2022).

# 22 DESIGN OF NI–FE HYBRID METAL HYDROXIDE NANOMATERIALS AS SELF-REPAIRING ANODE CATALYSTS FOR ALKALINE WATER ELECTROLYSIS

Ryuki Okada[1], Tatsuya Taniguchi[2], Yuta Sasaki[2], Yoshinori Nishiki[3], Zaenal Awaludin[3], Takaaki Nakai[3], Akihiro Kato[3], Shigenori Mitsusima[1], Yoshiyuki Kuroda[1]

[1]Grad. School of Eng. Sci., Yokohama Natl. Univ., 79-5 Tokiwadai, Hodogaya-ku, Yokohama 240- 8501, Japan
[2]Kawasaki Heavy Ind., Ltd., 1-1 Kawasakicho, Akashi, Hyogo, 673-8666, Japan
[3]De Nora Permelec, Ltd., 2023-15 Endo, Fujisawa, Kanagawa, 252-0816, Japan

**Keywords:** Alkaline water electrolysis, Renewable energy, Self-repairing catalyst, Nanosheet, Nanorod, OER activity

## INTRODUCTION

To use renewable energy efficiently, the conversion of renewable energy into hydrogen by alkaline water electrolysis has attracted much attention. When an alkaline water electrolyzer is powered by renewable energy, electrodes degrade due to reverse current generated on shutdown. To address this problem, we have reported the usefulness of a hybrid cobalt hydroxide nanosheet (Co-ns) as a self-repairing catalyst that keeps the oxygen evolution reaction (OER) ability under frequent potential fluctuations [1]. However, the OER activity of Co-ns is relatively lower than the state-of-the-art catalysts, such as Ni–Fe layered double hydroxides (LDHs). In this study, we synthesized hybrid Ni–Fe hydroxides with various compositions and structures, and their correlations with the OER activity.

## EXPERIMENTAL

Hybrid Ni–Fe hydroxides were synthesized by mixing nickel chloride, iron chloride, and tris(hydroxymethyl)aminomethane (Tris-$NH_2$) similar to the method to synthesize Co-ns [2]. Electrochemical measurements were performed in 1.0 M KOH, using a three-electrode cell made of PFA. A nickel plate, a nickel coil, and a reversible hydrogen electrode (RHE) were used as the working, counter, and reference electrodes, respectively. The chronoamperometry –0.5 V vs. RHE for 3 min was repeated to remove oxides from the Ni substrate surface. A dispersion of hybrid Ni–Fe hydroxide was added in the electrolyte to adjust the total metal concentration (Ni + Fe) at 40 ppm. Catalysts were deposited by repeating the constant current electrolysis at 800 mA $cm^{-2}$ for 30 min, cyclic voltammetries (CVs) and electrochemical impedance spectroscopy for the evaluation of OER activities for 8 times (total electrolysis time is 240 min).

## RESULTS AND DISCUSSION

The synthesis of hybrid Ni–Fe hydroxides were confirmed by XRD, FTIR, elemental analyses, and XAFS. The structures of products were layered, amorphous, and tunnel structures, depending on the metal composition (represented by Ni/(Ni + Fe)) and the degree of modification (represented by Tris-$NH_2$/(Ni + Fe)). Ni/(Ni + Fe) tends to be high when the concentration of metal salts was low and the concentration of Tris-$NH_2$ was high in the preparation solution. The oxidation states of Ni and Fe in all samples were +2.1 and +3.0, respectively.

The amount of catalyst deposited on the electrode by the electrolysis was confirmed by elemental analyses. The amount of deposited catalyst increased along with Ni/(Ni + Fe) (Fig. 1). The lowest deposition amount was 3 μg $cm^{-2}$ (Ni/(Ni + Fe)=0) and the highest one was 42 μg $cm^{-2}$ (Ni/(Ni + Fe)=0.82), whereas the values were still lower than that of Co-ns (90 μg $cm^{-2}$). In our previous study, the oxidation of $Co^{2+}$ to $Co^{3+}$ on an electrode surface is crucial for the electrochemical deposition of Co-ns[3]. Thus, it is reasonable that the content of divalent cation ($Ni^{2+}$) is related with the deposition amount.

From the OER measurements, the mass activity of catalysts was defined as the current at 1.53 V vs. RHE normalized by the amount of deposited catalyst ($i_{m,1.53}$). $i_{m,1.53}$ decreased along with the increase in Ni content (Fig. 2). The increase in Ni content is beneficial to the electrochemical deposition, though it is negatively correlated with the OER activity. Therefore, there is a trade-off between the amount of deposited catalyst and mass activity. The highest geometrical OER current density was obtained for Ni/(Ni + Fe) = 0.82 and $i_{1.53}$ = 296 mA $cm^{-2}$ (Fig. 3). The deposited amount of catalyst significantly contributed to the highest activity of the electrode.

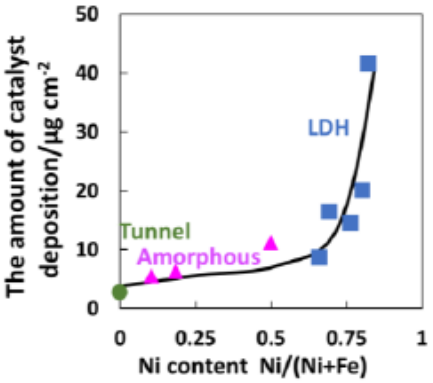


Fig.1. Catalyst loading as a function of Ni/(Ni+Fe)

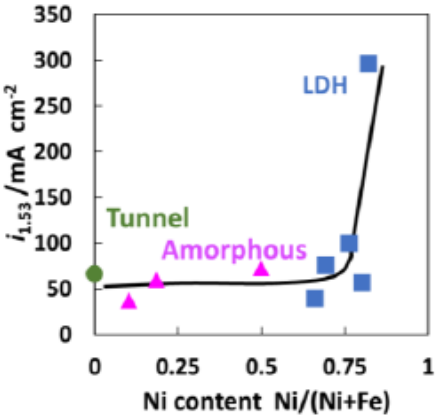


Fig.2. $i_{1.53}$ per Catalyst loading as a function of Ni/(Ni+Fe)

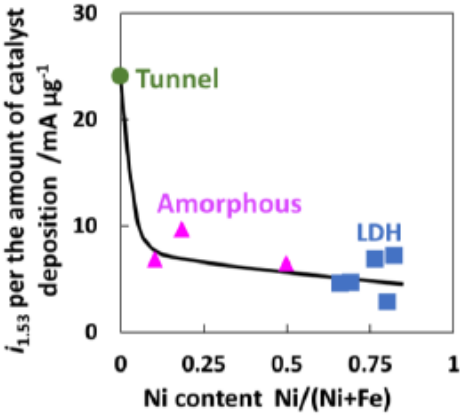


Fig.3. $i_{1.53}$ as a function of Ni/(Ni+Fe)

ACKNOWLEDGEMENT

Microscale droplets freezing was observed on wetting-patterned surfaces, and freezing propagation called ice bridge was visualized and measured.

REFERENCES

[1] Y. Kuroda et al., Electrochim. Acta, 323, 134812 (2019).
[2] Y. Kuroda et al., Chem. Eur. J., 23 (2017).
[3] R. Nakajima et al., ChemSusChem, e202300384, (2023)

# 23 CHARACTERIZATION OF ALKALINE WATER ELECTROLYSIS USING NI FOAM ELECTRODE

Kohsaku Okajima[1], Yoshiyuki Kuroda[1],and Shigenori Mitsushima[1.2]

[1]Graduate School of Engineering Science, Yokohama National University, 79-5 Tokiwadai, Hodogaya-ku, Yokohama 240-8501, Japan
[2]Institute of Advanced Sciences, Yokohama National University, 79-5 Tokiwadai, Hodogaya-ku, Yokohama 240-8501, Japan
e-mail: cel@ml.ynu.ac.jp

**Keywords:**. alkaline water electrolysis, foam electrode, mesh electrode

## INTRODUCTION

As a countermeasure to global warming, a shift to renewable energy sources that do not emit carbon dioxide is required. However, unevenly distributed over time and region makes difficulty to ensure a stable supply that meets demand. Therefore, research on water electrolysis technology to produce hydrogen using electricity derived from renewable energy sources has been attracting attention. Among these, alkaline water electrolysis (AWE) can use low-cost materials and can be easily scaled up. However, conventional design is not suitable for high current density operation compared with proton exchange membrane water electrolysis. In recent years, AWE design shifts from the conventional structure with a gap between the electrode and the diaphragm to a zero-gap structure where the mesh electrode and the diaphragm are in contact and expects to move to a porous electrode with a three-dimensional structure to achieve high current density for further cost reduction [1].
In this study, as a basic investigation of electrodes with a three-dimensional structure, cell voltage, bubble removal, and mass transfer characteristics of alkaline water electrolysis were analyzed using Ni foam electrodes with different pore diameters.

## EXPERIMENTAL

We utilized the forced-flow alkaline electrolyzer with the two types of Ni foams (pore size/thickness; 0.45 mm/1 mm(0.45), 0.85 mm/2 mm(0.85)) as anode and cathode, which also serves as electrolyte flow path. As shown in Figure 1, three types of electrode structures, three 0.45 foams stack (0.45×3), 0.45 and 0.85 foams stack (0.45+0.85), and 0.85 and 0.45 foams stack (0.85+0.45), were used for anodes or cathodes. Diaphragm was Zirfon®(AGFA, thickness 500 μm). Electrolyte is 7M KOH solution at 303 K in 0.1 MPa. After pre-treatment, the effect of flow rate on the activity was evaluated with Chronopotentiometry and Electrochemical Impedance Spectroscopy (EIS) in the current range from 0.01 to 3.5 A $cm^{-2}$ under anodes or cathodes flow rate 0.556, 5.56 cm/s and cathodes or anodes flow rate 5.56 cm/s. Internal resistance (Rint) was determined by high frequency intercept of EIS measurements. As a comparison, measurements were also made using a mesh electrode(30 mesh, thickness 0.3 mm).

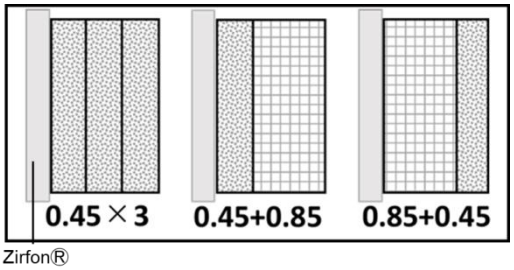

Fig.1 Electrode structures

## RESULTS AND DISCUSSION

Under anodic flow rate of 0.556, 5.56 cm/s with cathode of 0.45×3 and 5.56 cm/s. The iR free voltage was determined using the $R_{int}$ at a current density of 10 mA $cm^{-2}$, where the effect of mass transfer is small enough. Comparing the Ni foam with the mesh electrode, the foam electrodes clearly have lower cell voltages. This will be due to the large specific surface area of the porous electrode. In high current density region, Ni foam and mesh electrodes had almost same cell voltages. In this condition, the reaction would concentrate to the diaphragm side because of iR of electrolyte in electrode thickness direction. In these, 0.45+0.85 was the lowest cell voltage. Also, decrease in cell voltage due to increased flow rate was observed. For the cathode with 0.556, 5.56 cm/s, similar trend which 0.45+0.85 was the lowest cell voltage was observed, too. Here, the reduction in cell voltage dependent on anodes flow rate was greater than that on cathodes.

The effect of mass transfer was analyzed as shown in Fig. 3. The mass transfer overpotential; $E_{mass}$ was determined as the difference between iR free cell voltage which raw cell voltage minus resistance polarization and linear extrapolated line by the Tafel equation for the low current density region where there is no mass transfer effect. This $E_{mass}$ was used as an indicator of bubble removal.

Figure 4 shows the $E_{mass}$ as a function of current under anode flow rate of 0.556, 5.56 cm/s with cathode frow rate of 5.56 cm/s. The mesh electrode has a lower $E_{mass}$ in these electrodes. This may be due to accumulation of gas bubbles within the Ni foam, as this will decrease the effective surface area and prevent mass transport [2]. In the foam electrodes, the 0.45+0.85 was the lowest $E_{mass}$. The 0.45+0.85 showed superior bubble ejection compared to other structures. For the cathode with 0.556, 5.56 cm/s, similar trend which the 0.45+0.85 was the lowest $E_{mass}$ was obtained too. Here, the $E_{mass}$ of the cathode is smaller than anode. This may be attributed to the fact that oxygen bubbles have poorer bubble removal than hydrogen bubbles. It is thought that the size of the oxygen bubbles affects mass transfer more than the hydrogen, which is generated twice as much.

As described above, the 0.45+0.85, which is small pore size foam with large specific surface area on the diaphragm side and a large pore size foam with good bubble removal on the back of the diaphragm is lowest cell voltage. In fact, the result of image analysis had been shown that the size of oxygen bubbles is about twice as large as that of hydrogen bubbles in 25 wt% KOH solution [3].

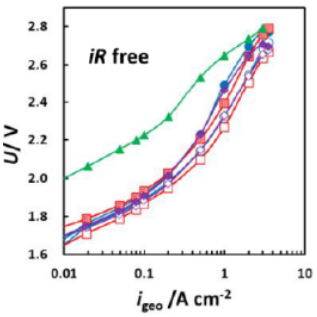


Fig.2 Cell voltage as a function of current. open: 5.56 cm/s, close: 0.556 cm/s ○, ●: 0.45×3, □, ■: 0.45+0.85, ◊, ♦: 0.85+0.45, ▲:mesh

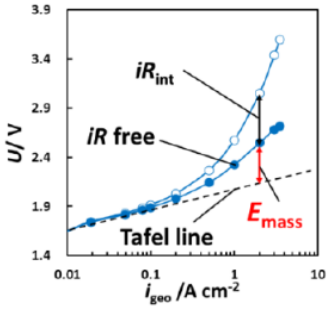


Fig.3 Analysis of mass transfer overpotential

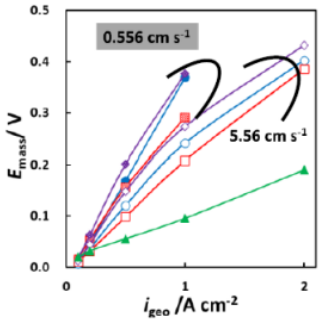


Fig.4 $E_{mass}$ as a function of current. ,open: 5.56 cm/s, close: 0.556cm/s,○, ●: 0.45×3, □, ■: 0.45+0.85, ◊, ♦: 0.85+0.45 ▲:mesh

REFERENCES

[1] Robert Phillips, Adam Edwards, Bertrand Rome, Daniel R. Jones, Charles W. Dunnill, Int. J. Hydrog. Energy,42, 23986- 23994(2017).

[2] Fernando Rocha, Renaud Delmelle, Christos Georgiadis, Joris Proost, J. Environmental Chemical Engineering, 10, 107648(2022)

[3] H. Matsushima, Y. Fukunaka, K. Kuribayashi, Electrochimica Acta, 51, 4190-4198(2006)

# 24 A MULTI-OBJECTIVE OPTIMIZATION APPROACH FOR THE DESIGN OF ALTERNATIVE PORT ENERGY SYSTEMS

Davide Pivetta[1], Rodolfo Taccani[2]

[1]Department of Engineering and Architecture, University of Trieste, Via Valerio 10, 34127 Trieste, Italy
[2]Department of Engineering and Architecture, University of Trieste, Via Valerio 10, 34127 Trieste, Italy
e-mail: davide.pivetta@phd.units.it

**Keywords:** water electrolysis, hydrogen carrier, industrial port area, port decarbonization, MILP approach, energy system optimization

The shipping and port industries are responsible of air and water pollution with serious effects on health of people living in port cities and coastal areas. Ship traffic is the primary source of gaseous emissions, accounting for over 70% of total emissions, while the remainder is generated by port equipment, buildings, and other industrial sectors linked to port-related activities [1]. Industrial Port Areas (IPAs) encompass ports and related industries, with ports historically serving as trade facilitators and suppliers of energy and materials [2]. Green hydrogen can play a key role for coupling different industrial and mobility sectors, such as maritime, cargo handling equipment, cruise-based-tourism, bulk distribution and transformation, thermal power plants, electricity grid operators and offshore wind, which are typically hosted in port areas [3]. The hydrogen uses as feedstock, energy carrier and fuel for both industry and port users could lead to a relevant reduction of emissions.
Although port decarbonization is a topic of great interest in the fields of energy and environmental engineering [4], there is a lack of comprehensive studies that analyse and synthesize the various energy demands (mechanical, electrical, heating, and cooling) of IPAs. Moreover, the design and optimization of alternative energy systems for ports are often overlooked at the global system level. To contribute to this framework and considering the environmental targets set by the Port of Singapore considered here as case study, this work proposes the estimation of typical energy demands and associated carbon dioxide equivalent ($CO_2$,eq) emissions of: port warehouses and buildings, tugboats, yard tractors and cranes operating in port, and a Combined Cycle Gas Turbine (CCGT) power plant. The energy and hydrogen demands are representative of the typical energy needs of a large Asian port located in a tropical area and a potential hydrogen demand of co-located power plants or heavy industries (i.e. steel, chemical and refining industries), whose decarbonization process may require green hydrogen in the future. Fig. 1 represents a simplified schematic of the proposed energy system configuration for the decarbonization of the IPA. A set of different energy solutions and energy system configurations has been proposed to meet the IPA energy demand at a reduced $CO_{2,eq}$ emissions. In particular, the exploitation of local RESs, electric and thermal energy storage systems, and technologies for hydrogen import/production, storage and utilization have been investigated. Furthermore, the model comprises also technologies to convert Liquid Organic Hydrogen Carriers (LOHC), ammonia ($NH_3$) and Liquefied Hydrogen ($LH_2$) into hydrogen to be used in power plant and for hybrid hydrogen vehicles. A multi-objective approach has been adopted through a Mixed-Integer Linear Programming (MILP) algorithm to concurrently optimize techno-economic and environmental objective functions. The results of the optimization are the optimal design and operation of energy conversion and storage units included in the system borders, represented

as a black dashed line. A sensitivity analysis is also performed on the parameters that most influence the optimisation results, such as the prices of imported hydrogen carriers and the alkaline electrolyser.

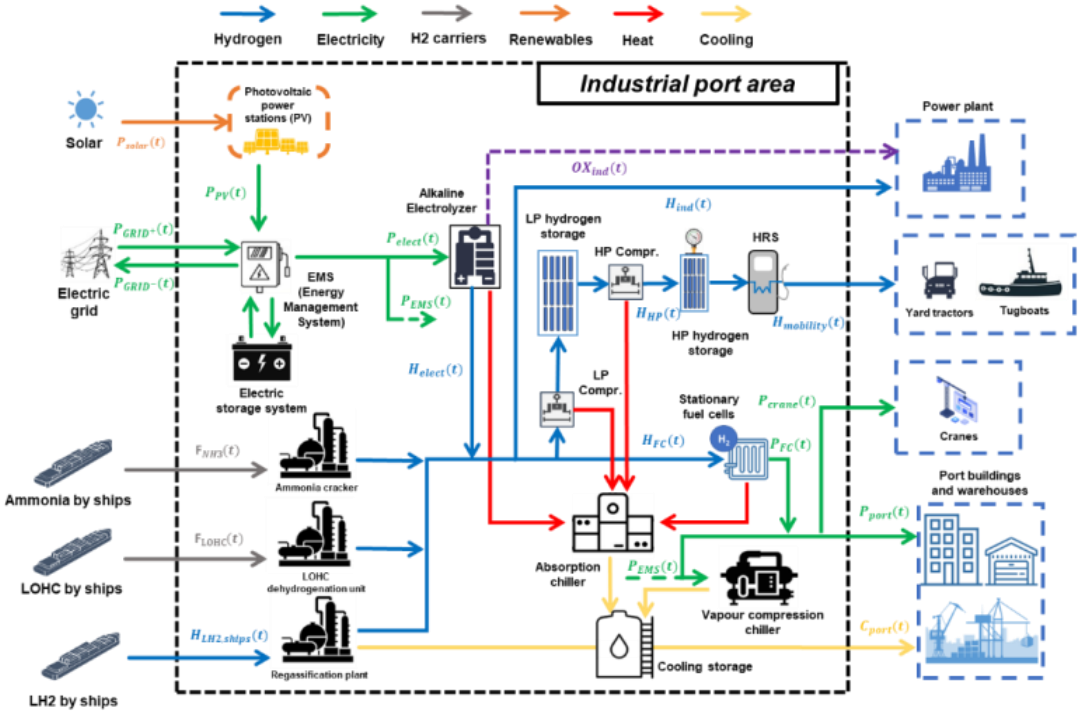


Figure 1: Simplified schematic of the energy system proposed for the analysed industrial port area of Singapore.

The operation of the CCGT power plant has a significant impact on the carbon emissions in the port area, accounting for 97.5% of the total carbon emissions. Hydrogen is a key element in decarbonization, especially when utilized by the CCGT power plant. This leads to a reduction in carbon emissions by up to 50%. Among the various hydrogen carriers, NH3 exhibits superior performance. LOHC and locally produced hydrogen are not economically feasible, hence, $NH_3$ is imported to satisfy more than 90% of the total hydrogen demand required by the CCGT plant, tugboats and yard tractors. $LH_2$ is imported for the remaining hydrogen demand, and the waste cold generated during $LH_2$ regassification is recovered and utilized to fulfil the cooling requirements of the port's buildings. The heating recovered from the hydrogen compressors could be efficiently used in an absorption chiller to meet a part of the cooling demand. Local hydrogen production by electrolysis is limited by the high cost of the electrolyser and the cost of electricity purchased from the grid, which is necessary to ensure a good utilisation factor for the electrolyser as the power available from photovoltaics is limited to a few hours during the day. Carbon tax ranging from 18 to 56 €/t$CO_{2,eq}$ does not affect the optimal design and operation of the system, while total emissions of the different configurations vary by about 2%. Other form of financial support should be evaluated to ensure the economic competitiveness of hydrogen technologies, such as electrolyzers and stationary fuel cells.

REFERENCES

[1] Rødseth KL, Schøyen H, Wangsness PB. Decomposing growth in Norwegian seaport container throughput and associated air pollution. Transp Res Part D Transp Environ 2020;85:102391. https://doi.org/10.1016/j.trd.2020.102391.

[2] Rodrigue J-P. Chapter 8.3 – Ports and Energy. Port Econ. Manag. Policy, n.d. https://doi.org/doi.org/10.4324/9780429318184.

[3] DNV GL. Ports: green gateways to Europe. 2022.

[4] Iris Ç, Lam JSL. A review of energy efficiency in ports: Operational strategies, technologies and energy management systems. Renew Sustain Energy Rev 2019;112:170–82. https://doi.org/10.1016/J.RSER.2019.04.069.

# 25 INVESTIGATIONS ON THE SYSTEM DESIGN OF ALKALINE DIRECT ETHANOL FUEL CELLS

Michaela Roschger[1], Sigrid Wolf[1], Andreas Billiani[1], Kurt Mayer[1], Maša Hren[2], Selestina Gorgieva[2], Boštjan Genorio[3], and Viktor Hacker[1]

[1]Institute of Chemical Engineering and Environmental Technology, Graz University of Technology, 8010 Graz, Austria
[2]Faculty of Mechanical Engineering, University of Maribor, 2000 Maribor, Slovenia
[3]Faculty of Chemistry and Chemical Technology, University of Ljubljana, 1000 Ljubljana, Slovenia
e-mail: michaela.roschger@tugraz.at

**Keywords:** membrane, ethanol oxidation reaction, oxygen reduction reaction, polarization curve, electrochemical impedance spectroscopy

## INTRODUCTION

The use of renewable, environmentally friendly, low toxic and liquid ethanol for power generation has received much attention in recent years. The ethanol, which is easy to transport and store, is for example converted electrochemically as a fuel in the alkaline direct ethanol fuel cell (ADEFC). However, ethanol is currently not completely cleaved during the ethanol oxidation reaction (EOR) at the anode. Therefore, the fuel also consists in addition to ethanol of an alkaline solution (e.g. KOH) to have a large amount of $OH^-$ ions at the anode available for the EOR. Due to this addition, there are three possible operation modes for the ADEFC: either the use of an anion-exchange membrane (AEM) to conduct the $OH^-$ ions formed at the cathode additionally through the membrane, the use of a separator since KOH is available as electrolyte and thus the conductivity of $OH^-$ is thereby given, or the use of a cation-exchange membrane (CEM) to conduct the $K^+$ from the anode to the cathode and thereby close the circuit, as shown in Figure 1. [1-3]

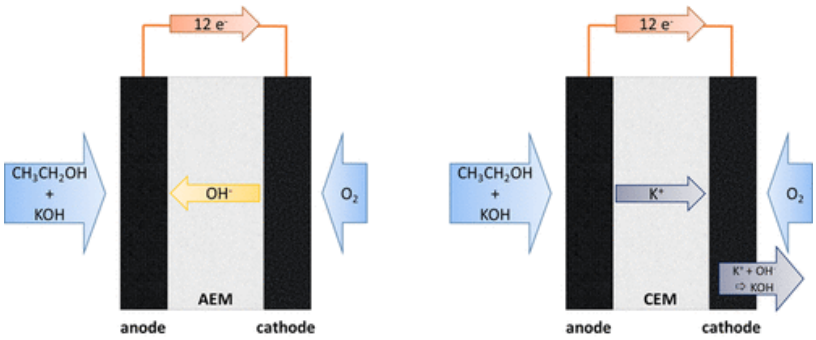


Anode reaction: $CH_3CH_2OH + 12\ OH^- \Rightarrow 2\ CO_2 + 9\ H_2O + 12\ e^-$
Cathode reaction: $3\ O_2 + 6\ H_2O + 12\ e^- \Rightarrow 12\ OH^-$

Figure 1: Schematic illustration of the different operation modes used (only AEM and CEM is shown) in the ADEFC (the graphic is taken without modification from our work [4]: ACS Omega 2023, 8, 23, 20845-20857. https://doi.org/10.1021/acsomega.3c01564 which was published under a CC BY 4.0 license (https://creativecommons.org/licenses/by/4.0/). Copyright © 2023 The Authors. Published by American Chemical Society).

Therefore, in this study the impact of a commercial AEM, a CEM and a microporous separator (MS) on the performance output in the ADEFC and in addition, the effect of the commercially available ionomer (cation-exchange ionomer and anion-exchange ionomer) in the catalyst layer was evaluated. Thus, the advantages and disadvantages of the respective operating mode could be clearly demonstrated.

## EXPERIMENTAL

The chemical and thermal stability, the ionic conductivity and the ethanol permeability of the membranes and the separator (AEM: Fumasep FAA-3-50, CEM: Nafion 212 and MS: Fumasep FAAM-40) were analysed first ex-situ for their application in the ADEFC as described in ref. [4]. For the single cell tests, membrane electrode assemblies (MEAs) were prepared: they consisted of the anodic electrode (PdNiBi/C catalyst [5] with a loading of 0.5 mg $cm^{-2}$ on carbon cloth) and the cathodic electrode (Ag-$Mn_xO_y$/C catalyst [5] with a loading of 0.25 mg $cm^{-2}$ on carbon paper) and the AEM, CEM or MS. For the preparation of the catalyst layer an ultrasonic spray coater was applied and either the Nafion ionomer (NS-5, PFSA 5%) or the Fumion ionomer (10 wt % in NMP) were utilized in the catalyst inks with the same I/C ratio. The AEM and the CEM were pre-treated in 1 M KOH for 24 h, whereas the MS in 6 M KOH. The polarization curves and electrochemical impedance spectra were recorded during continuous supply of 5 M KOH + 3 M EtOH at the anode and oxygen at the cathode. The surface morphology of the electrodes produced with the different ionomers was investigated with scanning electron microscopy. [4]

## RESULTS

The AEM exhibited high conductivity of $OH^-$ ions but poor thermal and chemical stability, due to degradation of the quaternary ammonium groups. The MS does not possess these groups and therefore showed high stability, but no intrinsic $OH^-$ conductivity. The use of the CEM was not advantageous, since the poor $K^+$ conductivity and its electroosmotic drag direction lead to a high ethanol crossover rate and performance losses. Thus, among the three different samples tested, the MS was the most promising. In contrast, however, higher cell performance was achieved with the Nafion ionomer, due to the better mass transport characteristics of the catalyst layer. Thus, a maximum power density of 79.4 mW $cm^{-2}$ at 80 °C could be obtained. [4]

## ACKNOWLEDGEMENT

The authors acknowledge the financial support by the Austrian Science Fund (FWF): I 3871-N37.

## REFERENCES

[1] L. An and T.S. Zhao: Energy Environmental Science, Vol. 4 (2011), p. 2213-2217
[2] L. An, T.S. Zhao, Q.X. Wu and L. Zeng: International Journal of Hydrogen Energy, Vol. 37 (2012), p. 14536-14542
[3] J. Huang and A. Faghri: Journal of Fuel Cell Science and Technology, Vol. 11 (2014), p. 051007
[4] M. Roschger, S. Wolf, A. Billiani, K. Mayer, M. Hren, S. Gorgieva, B. Genorio and V. Hacker: ACS Omega, Vol. 8 (2023), p. 20845-20857
[5] M. Roschger, S. Wolf, K. Mayer, A. Billiani, B. Genorio, S. Gorgieva and V. Hacker: Sustainable Energy Fuels, Vol. 7 (2023), p. 1093-1106

# 26 EFFECT OF EW OF PEM ON DIRECT TOLUENE ELECTRO-HYDROGENATION

Rio Shinohara[1], Kaoru Ikegami[2], Kensaku Nagasawa[3], Yoshiyuki Kuroda[1,2]
and Shigenori Mitsushima[1,2]

[1]Graduate school of Engineering Science, Yokohama National University, 79-5 Tokiwadai, Hodogaya-ku, Yokohama 240-8501, Japan
[2]Institute of Advanced Sciences, Yokohama National University, 79-5 Tokiwadai, Hodogaya-ku, Yokohama 240-8501, Japan
[3]Renewable Research Center, National Institute of Advanced Industrial Science and Technology, 2-2-9 Machiikedai, Koriyama 963-0298, Japan
e-mail: chemicalenerrgylaboratory-all@ynu.ac.jp

**Keywords:** direct toluene electro-hydrogenation, EW (equivalent weight), drag water

## INTRODUCTION

The organic chemical hydride is attracting attention as a technology for mass storage and transportation of renewable energy, which is unevenly distributed over time and region. The toluene (TOL) / methylcyclohexane (MCH) system is particularly advantageous in terms of safety and utilization of existing infrastructure compared to other energy carriers such as liquefied hydrogen and ammonia [1]. Our laboratory has been working on direct TOL electro-hydrogenation electrolyzer that simultaneously performs TOL hydrogenation and water electrolysis using proton exchange membrane (PEM) electrolysis [2]. The problem with using PEM is that the $H^+$ accompany water from the anode to the cathode, which is called drag water, causing the water to stagnate in the cathode catalyst layer and inhibiting the TOL supply. In this study, we have investigated the effect of equivalent weight (EW) of PEM on the amount of drag water and current efficiency of electrohydrogenation.

## EXPERIMENT

Table 1 summarize properties of used PEMs. A DSE® (De Nora Permelec, Ltd.) for the oxygen evolution was used as the anode. Carbon paper (39BB, SGL carbon Ltd.) loaded with 1 mg-PtRu $cm^{-2}$ of PtRu/C (TEC61E54, Tanaka Kikinzoku Kogyo) was used as the cathode with the same EW ionomer (I/C=0.8) The carbon paper, which also serves as the cathode reactant flow channel, was preloaded with 0.02 mg $cm^{-2}$ of Pt catalyst for chemical hydrogenation. The cathode was hot-pressed at 3.96 MPa for 10 min on the PEM at 190 °C except at 120 °C for M1100 and to fabricate a membrane cathode assembly.
The anode and cathode compartments were circulated 1 M (=mol $dm^{-3}$) $H_2SO_4$ and 10% TOL/MCH under 60 °C, respectively. Current efficiency that is the current ratio of TOL hydrogenation in whole current was determined by Faraday's law from the volume ratio of $H^2$ in the outlet TOL/MCH solution after 3 minutes of constant current electrolysis. In the water flux measurement, the amount of water in the cathode reservoir after constant current electrolysis was weighed.

Table.1 Characteristics of the used membrane

| Types | EW [g mol-1] | Side chain structure | Thickness [µm] |
|---|---|---|---|
| M1100 | 1100 | LSC | 127 |
| M950 | 950 | SSC | 50 |
| M720 | 720 | SSC | 100 |

## RESULTS AND DISUCUSSION

Figure 1 shows the dependence of the water flux from anode to cathode on the *EW*. The water flux of the M1100 was the highest and that of M950 was the lowest in these. The flux seems to decreased with the decrease of the *EW*, but side chain structure and thickness of the membrane may also affect to the flux and a clear dependence of the flux on the *EW* could not be confirmed. To exact discussion, the flux should be decompose electroosmosis and back diffusion factors.

Figure 2 shows the current efficiency as a function of current density. The M950 showed the highest current efficiency in these. The suppression of water transportation from anode to cathode would be an important factor to the increase in current efficiency. But the extremely low current efficiency of the M720 could not be explained. We would like to confirm the reproducibility of this phenomenon and clarify the effect of side chain structure on the current efficiency.

Not only the membrane, but also the *EW* of the cathode ionomer may affect the result. The lower the *EW*, the greater the water content and the more water accumulates in the cathode catalyst layer. Therefore, the supply of TOL may be inhibited when the *EW* is too low.

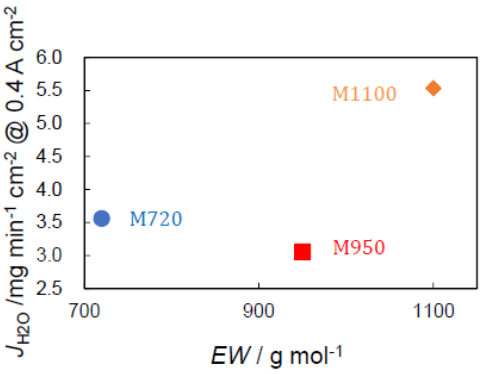


Fig.1 Relationship between EW and the amount of drag water

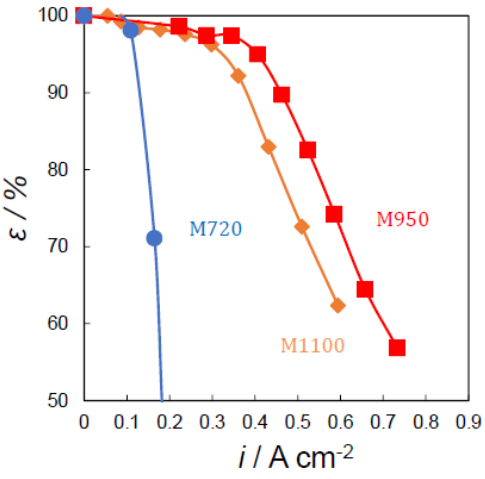


Fig.2 Current efficiency


## ACKNOWLEDGMENT

This study was supported by utilization project (JPNP14021) of the New Energy and Industrial Technology Development Organization (NEDO) in Japan. The electrode of Anode was supplied by De Nora Permelec Ltd. We appreciate the person concerned them.


## REFERENCES


[1] Agung Tri Wijayanta, Takuya Oda, Chandra Wahyu Purnomo, Takao Kashiwagi and Muhammad Aziz, Int. J. Hydrogen Energy, 44, 15026-15044, (2019)

[2] K. Nagasawa, Y. Sawaguchi, A. Kato, Y. Nishiki, S. Mitsushima, Electrochemistry, 86,339-344, (2018)

# 27 TOWARDS CONFORMAL AND FLUORINE-FREE COATINGS ON CARBON FIBER SUBSTRATES FOR POLYMER ELECTROLYTE FUEL CELLS

Irene Sinisgalli[1], Adrian Mularczyk[1], Antoni Forner-Cuenca[1]

[1]Electrochemical Materials and Systems, Department of Chemical Engineering and Chemistry, Eindhoven University of Technology, Eindhoven, Netherlands
e-mail: i.sinisgalli@tue.nl, a.a.mularczyk@tue.nl, a.forner.cuenca@tue.nl

**Keywords:** gas diffusion layer, water management, fluorine-free, electrografting, fuel cells

ABSTRACT

Decarbonizing the automotive sector has become a priority in the last decades and polymer electrolyte fuel cells (PEFCs) are a promising technology for the purpose, thanks to their high power, high efficiency, fast refilling and potentially zero emissions. In particular, PEFCs are well-suited for heavy-duty applications: they show unique scalability in terms of power and efficiency, and require a limited amount of infrastructures, as fewer refuelling stations are needed due to dedicated and predictable routes[1]. Nevertheless, to achieve reliable and cost-effective systems, existing challenges related to performance and durability need to be overcome. A powerful approach to improve these two is to optimize the water management, a complex but performance-defining issue[2]. Whilst the water generated during operation is beneficial to the membrane and the ionomer for proton conduction, it causes mass transport losses in the gas diffusion media by blocking the transport pathways for the reactant gases and limiting the overall performance of the system. State-of-the-art gas diffusion media are made by dip-coating carbon fiber-based substrates in a polytetrafluoroethylene (PTFE) dispersion. The treatment provides the material with the required hydrophobicity, but suffers from two major drawbacks. First, the PTFE coverage is heterogenous, resulting in uneven distribution of the wetting properties[3]. Second, the weak physical interactions between the substrate and the coating cause PTFE loss under operating conditions, negatively impacting both durability and performance[4]. Furthermore, efforts are being made to replace fluorine-containing materials, which are very prominent in PEFCs, because of the fluorine toxicity, that might result in a ban of per- and polyfluoroalkyl substances in 2024[5].
Our goal is to overcome the existing challenges through an alternative coating approach leveraging principles of liquid phase electrochemistry, electrografting. The proposed technique enables the formation of tuneable and conformal hydrophobic layers covalently bonded to the substrate[6,7], which we hypothesize would result in more stable and homogeneous coatings. Furthermore, given the large variety of molecules that can be grafted via this method, we foresee a pathway for the development of fluorine-free coatings. In the poster, I will first discuss our alternative synthetic approach to hydrophobize the fibrous substrates using fluorine-free molecules, such as silanes or siloxanes. Secondly, I will present the set of characterization techniques that we have used to assess critical properties of the functionalised materials. To conclude, I will discuss the performance of the novel gas diffusion layers in single-cell polymer electrolyte fuel cells. The ultimate goal of the research is to achieve advanced fluorine-free gas diffusion media with improved performance and durability.

ACKNOWLEDGMENTS

This project has received funding from the Fuel Cells and Hydrogen 2 Joint Undertaking (JU) under grant agreement No 101007170. The JU receives support from the European Union's Horizon 2020 research and innovation programme and Hydrogen Europe and Hydrogen Europe Research.

This project has received funding from the European Union's Horizon 2020 research and innovation programme under the Marie Skłodowska-Curie grant agreement No 899987 and the Eindhoven Institute for Renewable Energy Systems.

REFERENCES

[1] Cullen, D. A.; Neyerlin, K. C.; Ahluwalia, R. K.; Mukundan, R.; More, K. L.; Borup, R. L.; Weber, A. Z.; Myers, D. J.; Kusoglu, A. Nat Energy 2021, 6 (5), 462–474.

[2] Yue, L.; Wang, S.; Araki, T.; Utaka, Y.; Wang, Y. Int J Hydrogen Energy 2021, 46 (3), 2969–2977.

[3] Rofaiel, A.; Ellis, J. S.; Challa, P. R.; Bazylak, A. J Power Sources 2012, 201, 219–225.

[4] Pan, Y.; Wang, H.; Brandon, N. P. J Power Sources 2021, 230560.

[5] ECHA (European Chemical Agency), Restriction on the manufacture, placing on the market and use of PFASs , 2023, https://echa.europa.eu/-/echa-publishes-pfas-restriction-proposal.

[6] Bélanger, D.; Pinson, J. Chem Soc Rev 2011, 40 (7), 3995–4048.

[7] Thomas, Y. R. J.; Benayad, A.; Schroder, M.; Morin, A.; Pauchet, J. ACS Appl Mater Interfaces 2015, 7 (27), 15068–15077.

# 28 VISUALIZATION OF OXYGEN BUBBLES ON A FLAT IONOMER-COATED PLATINUM ELECTRODE

Hideki Suwa[1], Takuto Araki[2], Kohei. Toyama[3] and Sota. Kishi[4]

[1]Department of Mechanical Engineering, Yokohama National University, Kanagawa, Japan, suwa-hideki-jy@ynu.jp
[2]Faculty of Engineering, Yokohama National University, Kanagawa, Japan, taraki@ynu.jp
[3]Department of Mechanical Engineering, Yokohama National University, Kanagawa, Japan, toyama-kohei-cs@ynu.jp
[4]Department of Mechanical Engineering, Yokohama National University, Kanagawa, Japan, kishi-sota-mx@ynu.jp
e-mail: suwa-hideki-jy@ynu.jp

**Keywords:**.PEMWE, oxygen bubbles, oxygen transport, catalyst layer, ionomer, dissolved oxygen, SEM-EDX, high-speed camera

## INTRODUCTION

To improve the performance of polymer electrolyte membrane water electrolyzers (PEMWE), it is necessary to grasp oxygen transport from the reaction site. The main cause of efficiency loss in the high current density range is caused by the inhabitation of water supply, due to oxygen bubbles covering the catalyst surface [1]. In addition to that, increased oxygen activity on the surface of the catalyst layer can also reduce the electrolysis efficiency. Therefore, it is important to understand how the oxygen is transported near the reaction site in order to design an ideal catalyst structure. Our previous study has reported highly supersaturated dissolved oxygen and growing oxygen bubbles several tens of microns from the catalyst layer, confirming that the generated oxygen is transported in the dissolved state [2]. However, it has not been directly confirmed whether the generated oxygen can pass through the ionomer. In this study, oxygen bubbles were observed on the flat electrode in a simplified system of water electrolysis.

## EXPERIMENTAL

For the sake of visualization, a flat electrode was fabricated on a glass plate as shown Fig.1. The square reaction area was electroplated with Pt to create a catalyst surface, and the ionomer was spin-coated to completely cover the catalyst surface.

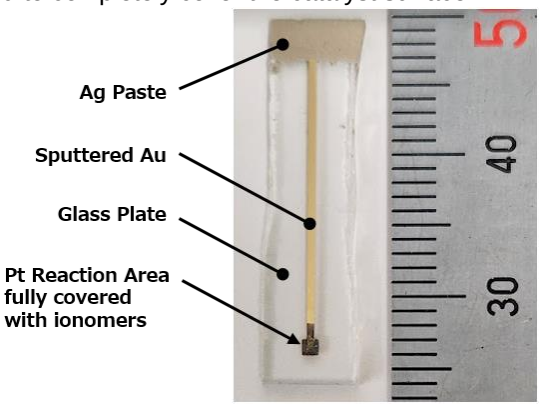


Fig. 1 Image of the electrode.

This electrode was used as the working electrode and the oxygen bubbles during electrolysis were observed with a high-speed camera. After electrolysis, the ionomer surface was observed using SEM-EDX.

## RESULTS AND DISCUSSION

Fig. 2 (a) shows the oxygen bubbles during electrolysis at 1.6 V. Oxygen bubbles are unbiasedly generated from above the reaction zone of the electrode. Since no behaviour was observed that was hindered by the ionomer membrane, it is assumed that oxygen bubbles are generated from the surface of the ionomer membrane. Fig. 2 (b) shows the element mapping of fluorine after electrolysis. It shows that there are no significant damages or cracks. These results indicate that oxygen bubbles do not destroy the ionomer and pass through it as dissolved oxygen.

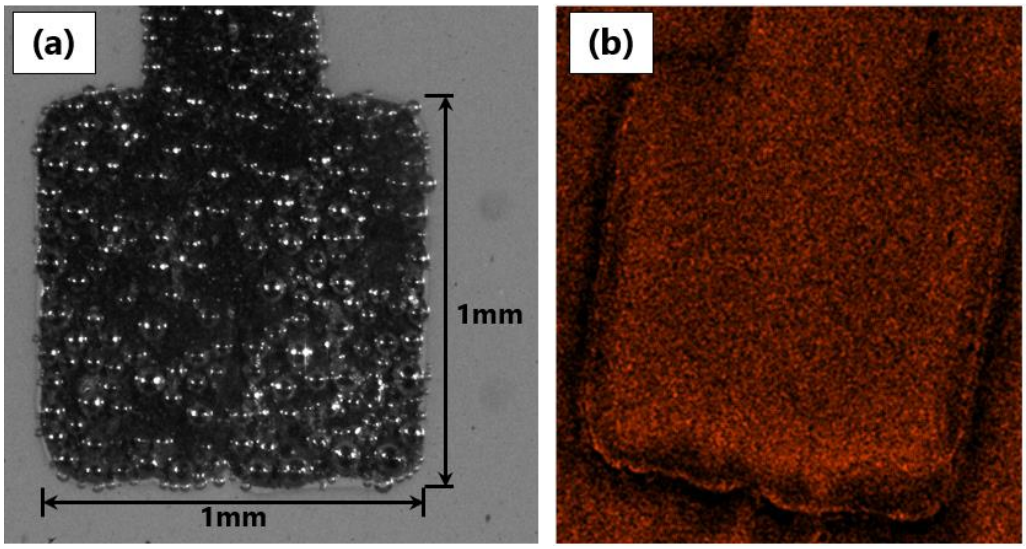


Fig. 2 (a) Image of oxygen bubbles during electrolysis, (b) Element mapping of fluorine after electrolysis.

## CONCLUSION

Oxygen bubbles near the ionomer and the surface of ionomer after electrolysis were observed. According to the images of oxygen bubbles during electrolysis and the element mapping of the electrode after electrolysis, oxygen generated from the catalyst surface formed into bubbles on the surface of the ionomer. This suggests that oxygen in the catalyst layer is transported through the water inside the ionomer. These results provide a new way of thinking in designing the ideal catalyst layer structure.

## REFERENCES

[1] P.J. Kim, CH. Lee, K.F. Fahy, and A. Bazylak: J. Electrochem. Soc., Vol. 167, (2020), 124522

[2] K. Watanabe, K. Wakuda, K. Wani, T. Araki, K. Nagasawa, and S. Mitsushima: J. Electrochem. Soc., Vol.169, Issue 4, (2022), 044515

# 29 ACTIVITY EVALUATION METHOD OF POWDER ELECTROCATALYST FOR GAS EVOLUTION REACTION

Yu Takenaga,[1] Kunpeng Li,[2] Kensaku Nagasawa,[3] Yoshiyuki Kuroda,[1,2] and Shigenori Mitsushima[1,2]

[1]Graduate School of Engineering Science, Yokohama National University, 79-5 Tokiwadai, Hodogayaku, Yokohama 240-8501, Japan
[2]Institute of Advanced Sciences, Yokohama National University, 79-5 Tokiwadai, Hodogaya-ku, Yokohama 240-8501, Japan
[3]Fukushima Renewable Energy Institute, National Institute of Advanced Industrial Science and Technology, 2-2-9 Machiikedai, Koriyama, Fukushima 963-0298, Japan
e-mail: ynugr-cel@ynu.ac.jp

**Keywords:**. alkaline water electrolysis, oxygen evolution reaction, powder electrocatalyst, activity, evaluation method

## INTRODUCTION

In recent years, efforts have been made to develop high activity and durability of electrocatalysts for water electrolysis. However, bubbles accumulate in the catalyst layer at high current density. This makes it difficult to accurately evaluate the catalyst activity, so that it is an important issue to separate the generated bubbles from the surface of the catalyst. Controlling the behaviour of generated bubbles by forced flow of electrolyte solution is a promising approach. This makes it possible to evaluate catalyst activity with gas generation reaction while suppressing additional equipment investment and/or heat treatment of the catalyst [1,2].
Therefore, in this study, we used an electrolytic single cell in which a powder catalyst is supported on a diaphragm and electrolyte forced flow. To develop an electrochemical method to evaluate the activity of powder catalysts for gas evolution reaction in a practical high current density range, we have analysed transition current of chronoamperometry (CA) to get oxygen bubble free current using forced flow cell.

## EXPERIMENTAL

1 $cm^2$ electrolyzer with an independent effective area contact control system was used. Figure 1 shows a schematic diagram of the catalyst fastening section of that electrolyzer. A catalyst was fastened between a diaphragm membrane and a rib of the current corrector, and electrolyte flowed through catalyst layer in interdigit forced flow field.

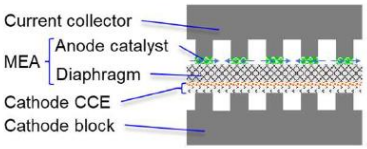

Fig. 1. Fastening part of the electrolyzer

PdH references were placed on the membrane by the contact with 7 M KOH, and potential was indicated based on reversible hydrogen electrode. The anode current collector is made of Pt-plated Ti. The anode and the cathode electrocatalyst are$LaNiO_3$ (LNO, 98.5 wt%, particle size 104 nm, 80.1 mg-LNO/$cm^2$, self-made by sol-gel method), and Pt/C (TKK). The anode catalyst was coated with the shape of the rib of 1 mm width rectangular array onto Zirfon membrane, and the cathode catalyst was coated onto a carbon paper (39BC, SGL) as cathode electrode. The loading amount of catalyst was analysed by XRF before electrochemical measurements.

The operation temperature was 30 °C and the electrolyte was 7 M KOH, circulating at 100 and 30 mL $min^{-1}$ in the working and counter electrode chambers, respectively. After chronopotentiometry (CP) at 1 A $cm^{-2}$ as a pretreatment, electrochemical measurements were made at CA. OER was evaluated by potential step from 1.50 V for 360 s of potential hold to the measured potential in the rage from 1.51 to 1.80 V for 10 s. The electrochemical impedance spectroscopy (EIS) was performed to evaluate internal resistance.

The current in CA decays with time. If the current decay is dominated by diffusion according to the Cottrell equation, inverse of current is linear relation to squire root of time with intercept of inverse of kinetic current where $i_k$: kinetic current density, $i_d$: diffusion-limited current density, F: Faraday constant, C: substrate concentration, D: diffusion coefficient. All except time t in the second term could be treated as constants. Therefore, the inverse of the measured current is linear to the square root of time, and the inverse of kinetic current is obtained from time zero extrapolated the inverse of the measured current as a function of square root of time [3,4].

$$1/i = 1/i_k + 1/i_d = 1/i_k + (\pi t)^{1/2}/\left(nFCD^{\frac{1}{2}}\right) \qquad (1)$$

## RESULTS AND DISCUSSION

Figure 2 shows the plots of the square root of time versus the relative of the reciprocal current density with 100 ms as the reference. If the current decrease like as Cottrell equation, the current shows linear region later than the completion of charging of the electric double layer of a few ms, but clear linear region was not observed at any potential. At the initial period of current decrease would be affected by supersaturation near the catalyst, and the second region would be affected by bubbles formation, which follows the same analogy as diffusion and follows equation (1). After the second region, the current becomes steady state [4]. Therefore, we thought it necessary to quantitatively define the initial stage of the second region where only the effect of bubble formation can be considered.

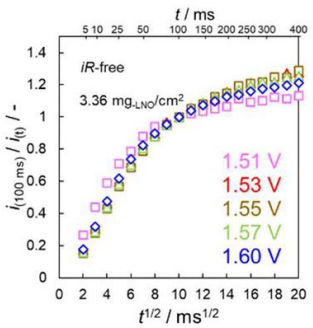


Fig. 2. The relative reciprocal current density as a function of the square root of time for CA.

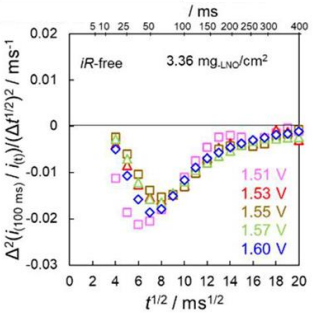


Fig. 3. The negative peak of the second-order derivative of the relative reciprocal current density per step potential.

To find the second region, the second-order derivative of Figure 2 is shown in Figure 3. A negative peak of the second-order derivative was observed for each potential, and the time domain of the peak was treated as the Cottrell equation like behavior. The kinetic current density was determined by extrapolating time zero from Figure 2.

Figure 4 shows the obtained polarization curves normalized the BET surface area of the LNO for various catalyst loadings. No significant dependence of I specific on the loading was observed and the Tafel slope was in the range from 57 to 68 mV/dec for 1.51 to 1.60 V, which is almost same as 40 to 100 mV/dec obtained by the ink application method with RDE [4, 5]. The evaluation range of current density in the conventional RDE method is 0.01 to 0.1 mA

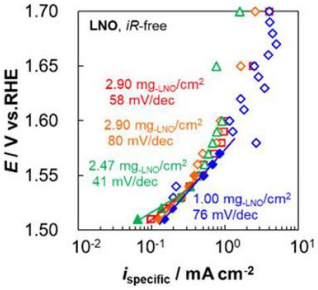


Fig. 4. Specific activity of $LaNiO_3$.

$cm^{-2}_{\text{-BET}}$ at 1.6 V [5]. On the other hand, this time zero analysis method reaches the same current density at 1.52 to 1.57 V. This would indicate that the suppression of OER activity by bubbles could be eliminated even it is difficult to evaluate the influence of generated gas bubbles to mass transfer or detachment of the catalyst, which makes difficulty to apply to durability evaluation using RDE [1]. Furthermore, the proposed method using time-zero analysis overcomes gas stagnation or catalyst detachment, and is expected to be applied to durability evaluation with accelerated durability testing (ADT) [7] and to activity evaluation of various catalysts.

ACKNOWLEDGEMENTS

This study was based on results obtained from the Development of Fundamental Technology for Advancement of Water Electrolysis Hydrogen Production in Advancement of Hydrogen Technologies and Utilization Project (JPNP14021) commissioned by the New Energy and Industrial Technology Development Organization (NEDO) in Japan.

REFERENCES

[1] H. A. El-Sayed, A. Weiß, L. F. Olbrich, G. P. Putro, and H. A. Gasteiger, J. Electrochem. Soc., 166, (8), 458-464, (2019).
[2] Y. Chen, J. Chen, K. Bai, Z. Xiao, S. Fan, J. of Power Sources, 561, 232733, (2023).
[3] K. Nagasawa, I. Matsuura, Y. Kuroda, S. Mitsushima, Electrochemistry, 90, 1, (2022).
[4] K. Nagasawa, L. Kunpeng, Y. Takenaga, Y. Kuroda, S. Mitsushima, Electrochemistry, 90, 4, (2022).
[5] Y. Tsukada, Y. Kuroda, H. Niiro, Y. Fujii, N. Fujimoto, S. Mitsushima, Electrochim. Acta., 353, 136544, (2020).
[6] S. Jung, C. C. L. McCrory, I. M. Ferrer, J. C. Peters, T. F. Jaramillo, J. Mater. Chem. A, 4, 3068-3076, (2016).
[7] A. Abdel Haleem, K. Nagasawa, Y. Kuroda, Y. Nishiki, A. Zaenal, S. Mitsushima, Electrochemistry, 89, 186-

# 30 VISUALIZATION OF MICROSCALE DROPLETS FREEZING ON HYDROPHILIC AND HYDROPHOBIC COMPOSITE SURFACES

Kohei Toyama[1], Takuto Araki[2]

[1]Grad. Sch. Of Eng. Sci., Yokohama National Univ., Tokiwadai 79-5, Hodogaya, Yokohama, Kanagawa, Japan, toyama-kohei-cs@ynu.jp
[2]Faculty of Eng., Yokohama National Univ., Tokiwadai 79-5, Hodogaka, Yokohama, Kanagawa, Japan, taraki@ynu.ac.jp
e-mail: toyama-kohei-cs@ynu.jp

**Keywords:** bubble detection, convolutional neural networks, data generation, deep learning, PEM water electlysis, difference images

## INTRODUCTION

Various fields, such as the paper industry, chemical engineering, and renewable energy, are faced with gas-liquid two-phase flows and are being studied by visualization and observation [1-3]. Although it is necessary to quantitatively evaluate the characteristics of bubbles, there is a limitation in the amount of labor required for detection and measurement by human observation of images. However, there are no examples for bubbles in polymer electrolyte membrane water electrolysis (PEMWE) cells, where the bubbles in PEMWE cells have heterogeneous backgrounds, unpatterned patterns, and unclear bubble contours. Existing methods for detecting these bubbles are not expected to be accurate enough. In this study, we developed a convolutional neural network (CNN)-based method to detect bubbles in PEMWE cells. Our method has two novel approaches: first, we developed an algorithm that automatically draws a pseudo-bubble image based on an actual bubble image on an arbitrary background as a method for automatically generating training data for the CNNs. Second, we developed a CNN-based bubble detection method that uses the motion of bubbles, specifically, the difference between the bubble image and the image from one frame ago, as input. Finally, we tested the algorithm on bubble images in a PEMWE cell and achieved an F1 score of 0.83 or better for all current densities of 0.5, 1, 2, and 3 A/cm2, and an F1 score of 0.844 for the entire detection.

## METHODS

To leverage the information regarding the "motion" of bubbles, we have developed a sophisticated bubble recognition system that simultaneously incorporates the difference image from the previous frame along with the bubble image. An overview of this system is depicted in Figure 1. It encompasses several key steps including bubble center detection, clustering, contour rendering, Hough transform, and reclustering. These steps collectively form a comprehensive pipeline for bubble recognition. To achieve this, we employ three distinct convolutional neural network (CNN) architectures: the Center classifier for bubble presence identification, the Center finder for accurate bubble center localization, and the Contour drawer for precise contour extraction. The architecture of the center finder and contour drawer (same structure) is shown in Figure 2. In addition, we have developed an algorithm that facilitates the creation of a simulated bubble by leveraging an actual bubble image. A comprehensive depiction of the step-by-step process involved in generating a singular bubble is presented in Figure 3. Finally, an algorithm was developed to automatically annotate the pseudo-bubble images. Figure 4 shows an example of automatically generated data.

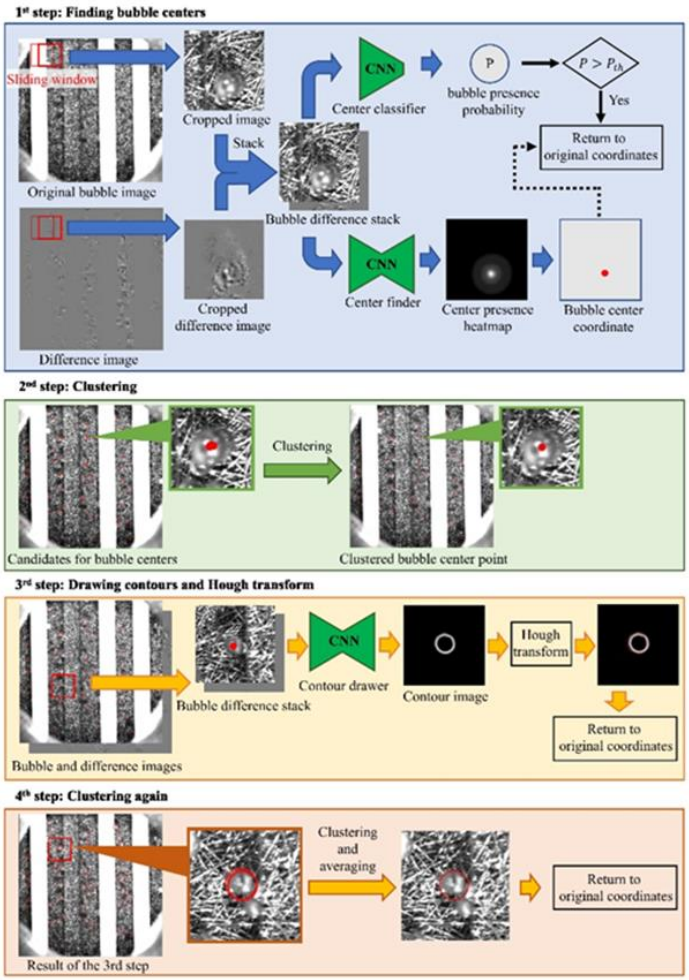


Fig. 1 Schematic diagram of bubble recognition flow

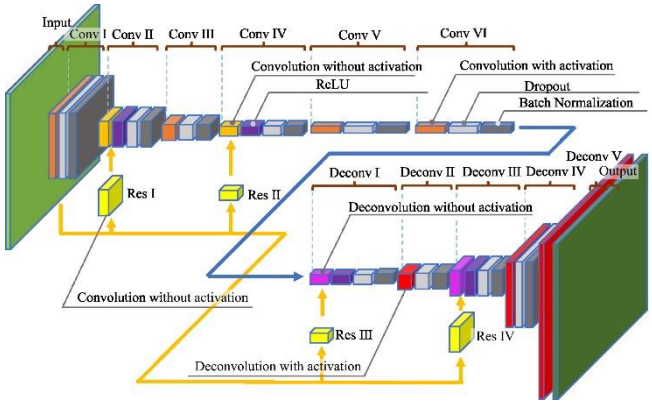


Fig. 2 Structure of Center finder and Contour drawer

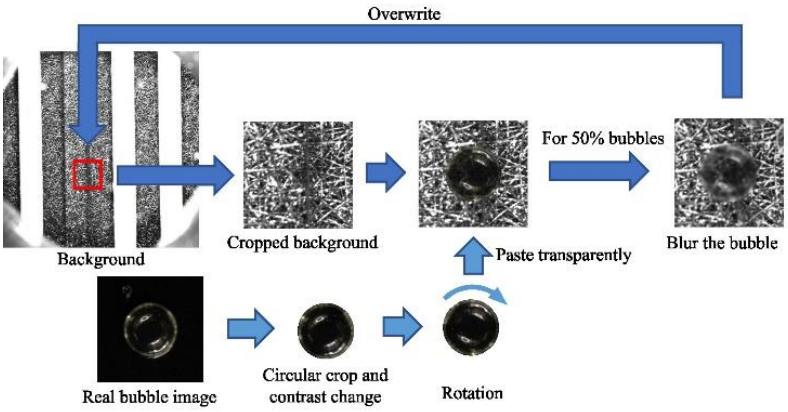


Fig. 3 Pseudo bubble drawing algorithm

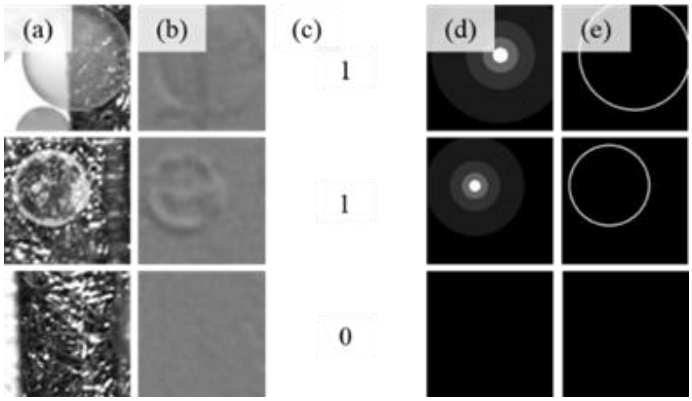


Fig. 4 Example of Ground Truth generated by the automatic annotation algorithm. Cropped (a) pseudo-bubble image and (b) pseudo-difference image. Ground Truth for (c) Center finder, (d) Center finder and (e) Contour drawer.

## RESULTS AND DISCUSSION

Bubble detection was conducted on the 2000th, 3000th, and 4000th frames of a high-speed movie captured at 4000 fps, depicting a PEM water electrolysis cell subjected to currents of 0.5, 1, 2, and 3 A/cm2. Notably, Figure 5(a) showcases a subset of the bubble detection outcomes, with the identified bubbles highlighted by red circles. To validate the accuracy of our model, we performed manual annotation of bubbles within the images, generating a test dataset. Subsequently, we calculated the confusion matrix for the results displayed in Figure 5(a) and visually represented it in Figure 5(b). Within this visualization, blue indicates true positives (correct detections), red corresponds to false negatives (missed detections), and yellow represents false positives (erroneous detections). True/false positives were determined based on whether the IoU (Intersection over Union) exceeded 0.5. In Figure 6, we present the goodness-of-fit rate (the probability of false positives), repeatability (the probability of false negatives), and F value (the harmonic mean of goodness-of-fit and repeatability) for each current dataset. For the entirety of our test data, we obtained a fit rate of 0.84, a repeatability of 0.77, and an F value of 0.81, affirming the attainment of a satisfactory level of accuracy. Additionally, we conducted bubble tracking and estimated the bubble generation rate based on the tracking outcomes. The bubble generation rate was further compared with the current (Figure 7) to elucidate potential correlations.

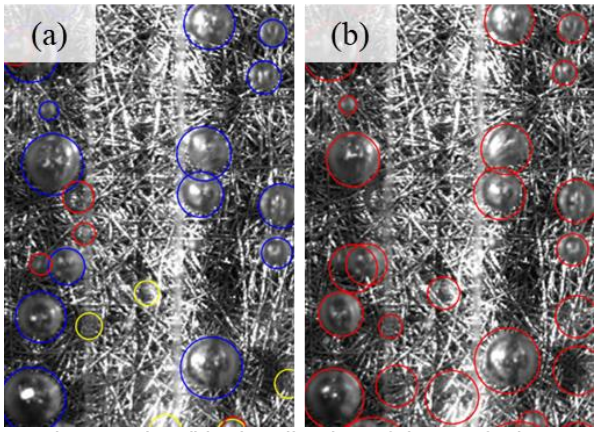


Fig. 5 (a) Bubble detection results. (b) Visualization of the confusion matrix of the detection results.

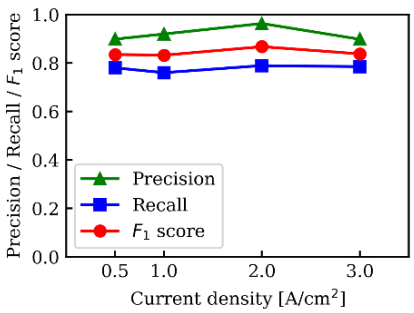


Fig.6 Precision, Recall and F1 score as a function of the current.

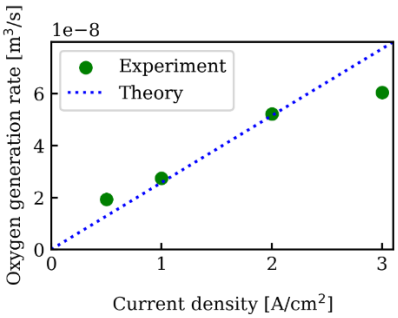


Fig. 7 Estimation of bubble generation rate by bubble tracking.

CONCLUSION

Detecting bubbles in PEM water electrolysis cells poses challenges due to the presence of inhomogeneous backgrounds and unclear contours, making conventional methods ineffective. In this research, we present a novel deep learning-based approach for bubble detection in PEM water electrolysis cells. Our method introduces two key contributions. Firstly, we have developed an algorithm that automatically generates a pseudo-bubble image on any given background using authentic bubble images. Secondly, we have devised a bubble detection technique that incorporates the difference from the previous frame along with the bubble image.

We conducted comprehensive bubble detection and verification experiments on images captured within a PEM water electrolysis cell. The detection process required approximately 1-2 minutes per image, which contained around 40 bubbles, utilizing a standard PC. The results of the verification process are as follows:

(1) Evaluation was performed for different current densities, yielding a compliance ratio of 0.89 or higher and an F value of 0.83 or higher across all conditions (0.5, 1, 2, and 3 A/cm2). The F value for the overall testing dataset reached 0.844.

(2) Further evaluation was conducted based on different bubble radii, demonstrating an F value exceeding 0.85 for bubbles with a radius of 15 pix (0.12 mm) or larger. For bubbles with

a radius below 45 pix (0.36 mm), the mean error remained below ±2.9 pix, with a standard deviation below 3.5 pix.

(3) The proposed method outperformed the model that did not incorporate difference images, improving the F value by 0.012. This outcome emphasizes the enhanced accuracy achieved by including difference images as input.

In conclusion, our deep learning-based bubble detection method shows promising results, surpassing conventional approaches by effectively addressing the challenges associated with background inhomogeneity and unclear contours in PEM water electrolysis cells.

REFERENCES

[1] J. Ilonen, et al., Pattern Recognit Lett (2018) pp.60-66
[2] Y. Cui, et al., Chem. Eng. J. 449 (2022) 137859
[3] K. Watanabe, J. Electrochem. Soc. 169 (2022) 044515

# 31 EFFECT OF PORE SIZE ON THE OXYGEN EVOLUTION REACTIONACTIVITY OF HYDROGEL ELECTRODES COMPOSED OF HYBRID COBALT HYDROXIDE NANOSHEETS

Hiroki Wago,[1] Tatsuya Taniguchi,[2] Yuta Sasaki,[2] Yoshinori Nishiki,[3] Zaenal Awaludin,[3] Takaaki Nakai,[3] Akihiro Kato,[3] Shigenori Mitsushima,[1,4] and Yoshiyuki Kuroda[1,4]

[1]Grad. School of Eng. Sci., Yokohama Natl. Univ., 79-5 Tokiwadai, Hodogaya-ku, Yokohama 240-8501, Japan
[2]Kawasaki Heavy Ind., Ltd., 1-1 Kawasakicho, Akashi, Hyogo, 673-8666, Japan
[3]De Nora Permelec, Ltd., 2023-15 Endo, Fujisawa, Kanagawa, 252-0816, Japan
[4]Adv. Chem. Energy Res. Center, Inst. of Adv. Sci., Yokohama Natl. Univ., 79-5 Tokiwadai, Hodogaya-ku, Yokohama 240-8501, Japan
e-mail: wago-hiroki-hp@ynu.jp

**Keywords:**.hydrogel electrode, alkaline water electrolysis, oxygen evolution reaction

## INTRODUCTION

Alkaline water electrolysis (AWE) is a promising technology for large-scale production of hydrogen from renewable energy; however, the sluggish oxygen evolution reaction leads to a large overvoltage. Porous electrodes with a large specific surface area are useful to achieve high current densities in AWE, whereas mass transport in small pores often reduces the overall current density. We have reported that hydrogel electrodes, possessing a flexible framework composed of interconnected hybrid cobalt hydroxide nanosheets (Co-ns), exhibit enhanced mass transport at high current density [1]. Hydrogel electrodes can be regarded as porous electrodes swollen by electrolytes. They are expected to repair cracked surfaces by recombination of microparticles and to optimize the framework structure suitable for mass transport (Fig. 1). In this study, we demonstrate the relationship between thepore size of the hydrogel electrodes and the OER activity at high current density.

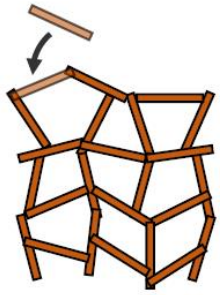

Fig. 1 Illustration of hydrogel electrodes repairing cracks.

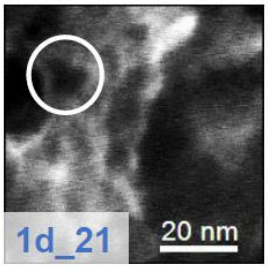


Fig. 2 FESEM images of dried hydrogel electrode.

## EXPERIMENT

Co-ns was synthesized by mixing aqueous solutions of 1.0 M tris(hydroxymethyl)aminomethane and 0.1 M $CoCl_2 \cdot 6H_2O$, followed by heating at 90 °C [2]. The heating time was varied as 1, 5 and 10 days to control the size. Electrochemical measurements were performed in a 1.0 M KOH aq., using a three-electrode cell made of PFA. Cons was dispersed in the electrolyte. Nickel plate, nickel coil, and reversible hydrogen electrode (RHE) were used as working, counter, and reference electrodes, respectively. Co-ns was deposited on the electrode by constant current electrolysis at 800 mA $cm^{-2}$ for varied time (10 min–100 h). The OER activity was evaluated by cyclic voltammetry (CV) and electrochemical impedance spectroscopy for iR correction.

## RESULTS AND DISCUSSION

TEM images of the synthesized Co-ns exhibited that the size of Co-ns increased along with the heating time. Therefore, the samples were named as 1d_21, 5d_34 and 10d_42, based on the heating time (days) and average size (nm). The FESEM images of the hydrogels after drying showed that nanosheets were assembled into house-of-cards structures (Fig. 2). The assembled structures of Cons with different diameters were analogous to one another.

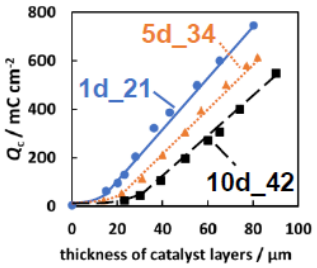


Fig. 3 Relationship between Qc and thickness of catalyst layers.

The charges of the cathodic peaks (Qc) at 0.8–1.5 V vs. RHE due to $Co^{2+/3+}$ and $Co^{3+/4+}$ in cyclic voltammograms were used as a measure of the amount of deposited Co-ns. The linear relationship between Qc and the thickness of catalyst layers exhibited that deposited Co-ns presented uniformly along the thickness of catalyst layers (Fig. 3). The slope of this line corresponds to the porosity of the hydrogels. The porosity increased along with the diameter of Co-ns; therefore, the pore size is expected to depend on the diameter of Co-ns because of the analogy of the assembled structure.

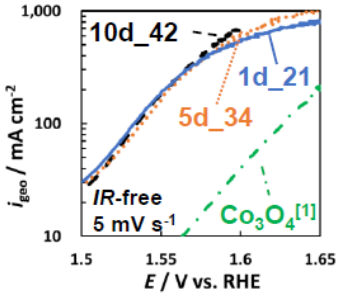


Fig. 4 Polarization curves of porous / hydrogel electrodes.

Polarization curves indicate the hydrogel electrodes achieves higher OER current density than a conventional porous electrode ($Co_3O_4$ [1]) (Fig. 4). OER current density at 1.6 V vs. RHE ($i_{geo\text{-}1.6\ V}$) was plotted as a function of thickness of catalyst layers, exhibiting a liner relationship, deviating from linearity with increasing the thickness of catalyst layers (Fig. 5). This indicates that OER current density is limited by the blockage of mass transport in the pores by generated gas molecules and OH–. The thicknesses of catalyst layers that deviated from this linear relationship were 40 µm for 1d_21, 60 µm for 5d_34, 90 µm for 10d_42, indicating the linear relationship between current density and the thickness of catalyst layers up to higher current density, along with pore sizes of hydrogels.

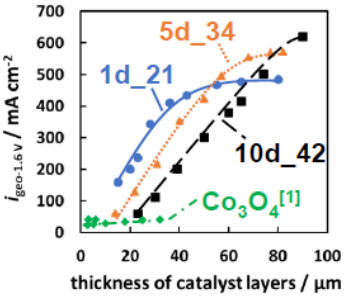


Fig. 5 Relationship between $i_{geo\text{-}1.6\ V}$ and thickness of catalyst layers

In conclusion, the size of Co-ns was used to control the porosity and pore size of hydrogel electrodes. Hydrogel electrodes with larger pore size exhibited better mass transport to achieve higher OER activity at high current density. These insights will contribute to designing an optimal hydrogel as an oxygen evolving electrode.


## ACKNOWLEDGEMENT

This work was supported partially by the JSPS K AKENHI from MEXT, Japan.


## REFERENCES


[1] R. Nakajima, T. Wago, T. Taniguchi, Y. Sasaki, Y. Nishiki, A. Zaenal, T. Nakai, A. Kato, S. Mitsushima, and Y. Kuroda, in preparation.

[2] Y. Kuroda, T. Koichi, K. Muramatsu, K. Yamaguchi, N. Mizuno, A. Shimojima, H. Wada, and K. Kuroda, Chem. Eur. J., 23 (2017) 5023.

# 32 INVESTIGATION OF EACH MEA COMPONENT'S IMPACT ON THE HT-PEMFC AND NUMERICAL MODELLING FOR AIRCRAFT APPLICATION

Ahyeon Won[1], Jens Tübke[1.2] and Carsten Cremers[1]

[1]Fraunhofer ICT, Department of Applied Electrochemistry, Joseph-von-Fraunhofer-Straße 7, 76327 Pfinztal, Germany
[2]Karlsurhe Institute of Technology, Institute for Mechanical Process Engineering and Mechanics, Straße am Forum 8, 76133 Kalsruhe, Germany
e-mail: ahyeon.won@ict.fraunhofer.de,

**Keywords:**.HT-PEMFC, MEA, aircraft, Ansys Fluent

Aviation sector is one of the industries with the fastest growth in greenhouse gas emissions [1]. In this sector, the polymer electrolyte membrane fuel cell (PEMFC) holds the most promise due to its relatively low operating temperatures with high energy density, and quick startup [2]. PEMFC is categorized as either low-temperature PEM (LT-PEM) or high-temperature PEM (HT-PEM) depending on the operating temperature. HT-PEMFC can be more in accordance with aircraft operation requirements than LT-PEMFC, regarding its lack of a water management system and better heat rejection.
However, there are few studies analysing the parameters affecting on cell performance and their interlace in HT-PEMFC. Thus, the impact of each MEA component should be comprehended by specific measurement techniques. This research will develop several MEAs with different components and conduct single cell tests at different working conditions to compare polarization curves. Additionally, cell degradation test, sensitivity analyses on water vapor and low stoichiometry, and electrochemical impedance spectroscopy will follow.

**Table 1. MEAs with variable components**

| | Membrane | Binder | Catalyst | GDL |
|---|---|---|---|---|
| MEA 1 | Celtec®-P | PTFE | Pt/C | SGL Sigracet |
| MEA 2 | Celtec®-P | PTFE | Pt/C | variable |
| … | … | … | … | … |
| MEA n | variable | variable | variable | variable |

Due to time and financial constraints, it is not possible to execute each experiment under a distinct set of settings. This issue can be resolved with the help of numerical simulations accompanied by real experiments. PEMFC model in Ansys Fluent software will be utilized in this study to simulate and it is expected to predict the polarization curve, fluid behaviour, thermal conductivity, and electric current [3,4]. According to the simulations, the optimized components and working conditions of PEMFC, in the view of air transport, can be discovered.

REFERENCES

[1] Reducing emissions from aviation. Climate Action. https://climate.ec.europa.eu/eu-action/transport-emissions/reducing-emissions-aviation_en

[2] Visvanathan, V. K., Palaniswamy, K., Ponnaiyan, D., Chandran, M., Kumaresan, T., Ramasamy, J., & Sundaram, S. (2023, March 15). Fuel Cell Products for Sustainable Transportation and Stationary Power Generation: Review on Market Perspective. Energies, 16(6), 2748. https://doi.org/10.3390/en16062748

[3] Simulating Proton-Exchange Membrane Fuel Cells using Non-Conformal Interfaces in Ansys Fluent. Ansys Innovation Space. https://www.ansys.com/training-center/course-catalog/fluids/simulating-proton-exchange-membrane-fuel-cells-using-non-conformal-interfaces-in-ansys-fluent#tab1-1

[4] Fuel Cell PEMFC in porous medium, ANSYS Fluent Training. MR CFD. https://www.mr-cfd.com/shop/fuel-cell-pemfc-cfd-simulation/

**Student Poster Presentation on**
**Hydrogen and Fuel Cells**

within the 15th International Summer School on Advanced Studies of Polymer Electrolyte Fuel Cells

August 30th 2023

Institute of Chemical Engineering
and Environmental Technology, NAWI Graz
Graz University of Technology,
Inffeldgasse 25c, 8010 Graz, Austria

https://www.tugraz.at/institute/ceet/home/

Editors: Viktor Hacker, Shigenori Mitsushima, Bernhard Gollas and Merit Bodner
Layout: Michael Lammer
Cover: Institute of Chemical Engineering and Environmental Technology/ TU Graz
2023 Verlag der Technischen Universität Graz
https://www.tugraz-verlag.at/
ISBN (e-book) 978-3-85125-973-5
DOI 10.3217/978-3-85125-973-5



Financial support was provided by the Austrian Ministry Climate Action, Environment, Energy, Mobility, Innovation and Technology, the Austrian Research Promotion Agency (FFG), the IEA Research Cooperation and TU Austria, the umbrella association of the Austrian Universities of Technology.